Engineering of conserved sequence motif 1 residues in halohydrin dehalogenase HheC simultaneously enhances activity, stability and enantioselectivity

Sophie Staar[a], Miquel Estévez-Gay[b], Felix Kaspar[a,c], Sílvia Osuna*[b,d], Anett Schallmey*[a,e,f]

[a] Sophie Staar, Dr. Felix Kaspar, Prof. Dr. Anett Schallmey
Institute for Biochemistry, Biotechnology and Bioinformatics, Technische Universität Braunschweig, Spielmannstr. 7, 38106 Braunschweig, Germany
[b] Dr. Miquel Estévez-Gay, Prof. Dr. Sílvia Osuna
Institut de Química Computacional i Catàlisi (IQCC), Departament de Química, Universitat de Girona, c/Maria Aurèlia Capmany 69, 17
003 Girona, Catalonia, Spain
[c] Dr. Felix Kaspar
Chair of Bioprocess Engineering, Institute of Biotechnology, Faculty III Process Sciences
Technische Universität Berlin
Ackerstraße 76, 13355 Berlin, Germany
[d] Prof. Dr. Sílvia Osuna
ICREA, Passeig Lluís Companys 23, 08010 Barcelona, Catalonia, Spain
[e] Prof. Dr. Anett Schallmey
Braunschweig Integrated Center of Systems Biology (BRICS), Technische Universität Braunschweig, Rebenring 56, 38106 Braunschweig, Germany
[f] Prof. Dr. Anett Schallmey
Center of Pharmaceutical Engineering (PVZ), Technische Universität Braunschweig, Franz-Liszt-Str. 35a, 38106 Braunschweig, Germany

* **Correspondence**
Prof. Dr. Anett Schallmey, Institute for Biochemistry, Biotechnology and Bioinformatics, Technical University Braunschweig, Spielmannstr. 7, 38106 Braunschweig, Germany.
E-mail: a.schallmey@tu-braunschweig.de

Prof. Dr. Sílvia Osuna, Institut de Química Computacional i Catàlisi (IQCC), Departament de Química, Universitat de Girona, c/Maria Aurèlia Capmany 69, 17003 Girona, Catalonia, Spain
E-mail: silviaosu@gmail.com

ABSTRACT

Halohydrin dehalogenases (HHDHs) are powerful enzymes for the asymmetric diversification of oxyfunctionalized synthons. They feature two characteristic sequence motifs that distinguish them from homologous short-chain dehydrogenases and reductases. Sequence motif 1, carrying a conserved threonine, glycine and a central aromatic residue, lines the nucleophile binding pocket of HHDHs. It could therefore impact nucleophile binding and presumably also activity of the enzymes. However, experimental evidence supporting this theory is largely missing. Herein, we systematically studied the mutability of the three conserved motif 1 residues as well as their resulting impact on enzyme activity, stability and selectivity in two model HHDHs: HheC from *Agrobacterium radiobacter* AD1 and HheG from *Ilumatobacter coccineus*. In both HheC and HheG, the conserved threonine and glycine only tolerated mutations to structurally similar amino acids. In contrast, the central aromatic (i.e., phenylalanine or tyrosine) residue of motif 1 demonstrated much higher variability in HheC. Remarkably, some of these variants featured drastically altered activity, stability and selectivity characteristics. For instance, variant HheC F12Y displayed up to 5-fold increased specific activity in various epoxide ring opening and dehalogenation reactions as well as enhanced enantioselectivity (e.g., an E-value of 74 in the azidolysis of epichlorohydrin compared to E = 22 for HheC wild type), while exhibiting also a 10 K higher apparent melting temperature. QM and MD simulations support the experimentally observed activity increase of HheC F12Y and revealed alterations in the hydrogen bonding network within the active site. As such, our results demonstrate that multiple enzyme properties of HHDHs can be altered through targeted mutagenesis of conserved motif 1 residues. In addition, this work illustrates that motif 1 plays vital roles beyond nucleophile binding by impacting solubility and stability properties. These insights advance our understanding of HHDH active sites and will facilitate their future engineering.

Keywords: halohydrin dehalogenase, protein engineering, epoxide ring opening, dehalogenation, spectrophotometric assay, quantum mechanics, molecular dynamics

INTRODUCTION

Halohydrin dehalogenases (HHDHs) have recently distinguished themselves as powerful enzymes for the asymmetric diversification of oxyfunctionalized synthons.[1–8] In nature, these bacterial lyases catalyze the reversible dehalogenation of *β*-haloalcohols through formation of the corresponding epoxides.[9] More importantly, they are capable of accepting a number of anionic *C*-, *N*-, *O*-, and *S*-nucleophiles in the reverse reaction, i.e. epoxide ring opening, giving access to a large repertoire of valuable products.[10] For instance, recent impressive biocatalytic examples for the application of HHDHs in asymmetric synthesis include the preparation of enantiopure *β*-nitroalcohols[11], and thiiranes[12], as well as the desymmetrization of 2-substituted-1,3-dichloro-2-propanols with subsequent cyanate-mediated ring opening to afford optically pure epoxides and oxazolidinones[1] among others.[7,13,14]

HHDHs share significant homology/similarity with short-chain dehydrogenases and reductases (SDRs) on the sequence, structural and mechanistic level as the result of a close phylogenetic relationship, although they catalyze entirely different chemical reactions.[15–17] Previously, this similarity has largely impeded a fast discrimination of HHDHs and SDR enzymes solely based on given protein sequences. With the discovery of HHDH-specific sequence motifs in 2014, database mining approaches facilitated the identification of novel HHDHs and yielded a plethora of new enzymes with partially unprecedented catalytic characteristics.[18–20] These HHDH sequence fingerprints include the N-terminal motif T-X_4-F/Y-X-G (motif 1), lining the nucleophile binding pocket of halohydrin dehalogenases, as well as the motif S-X_{12}-Y-X_3-R (motif 2), covering the catalytic residues serine, tyrosine and arginine.[15,17,21,22] For comparison, the corresponding sequence motifs of SDRs are T-G/A-X_3-G/A-X-G (motif 1)[16,18] and S-$X_{10\text{-}14}$-Y-X_3-K (motif 2),[16,17] respectively. In contrast to HHDHs, SDR motif 1 represents the typical glycine-rich nucleotide-binding sequence required for nicotinamide cofactor binding in those enzymes.[17]

While the mechanistic role of the three conserved catalytic residues serine, tyrosine and arginine (as part of motif 2) of HHDHs has already been elucidated using HheC from *Agrobacterium radiobacter* AD1 as a model enzyme,[15,17,21,22] the functional role and mutability of the conserved residues in motif 1 remains largely unexplored. Moreover, we hypothesized that HHDH variants with substantially improved biocatalytic performance could be accessed through engineering of motif 1 residues, as they should impact nucleophile binding. Crystal structures of HheC in complex with a bromide or chloride ion (PDB IDs 1PWX and 1PWZ, respectively) have demonstrated that the side chain of the central aromatic residue F12 in motif 1 forms a direct interaction with the negatively charged halide, which is tightly wedged between aromatic residues.[17] Such a direct interaction with the nucleophile, however, was not present in the crystal structure of HheB from *Corynebacterium* sp. strain N-1074 in complex with chloride (PDB ID 4ZD6), which carries a tyrosine at position 19.[23] Moreover, in a study by Wu *et al.* on the thermostabilization of HheC by combinatorial directed evolution, mutation F12Y was found to increase the enzyme's thermostability and yielded a 1.5-fold gain in specific activity in the dehalogenation of 1,3-dichloropropanol.[24] Similarly, mutations at the structurally equivalent position Y15 in *Ab*HheG from *Acidimicrobiia* bacterium yielded variants with improved enantioselectivity in the ring opening of styrene oxide with cyanate quite recently.[14] Both examples directly hint at the hitherto underexplored possibility to steer the catalytic properties of HHDHs via targeted mutagenesis of sequence motif 1.

Building on these precedents, we therefore set out to systematically engineer the conserved motif 1 residues in two representative HHDHs, HheC from *A. radiobacter* as well as HheG from *Ilumatobacter coccineus*. We selected these HHDHs based on their biocatalytic relevance,[4,10,13,20,25–28] the fact that both enzymes offer high-resolution crystal structures,[17,20,26] as well as their highly dissimilar catalytic properties. HheC is the by far best studied member of the HHDH family, generally displaying high catalytic activity and enantioselectivity in the dehalogenation of various substrates as well as in the ring opening of terminal epoxides.[3–5,15,29–33] Moreover, numerous protein engineering studies of HheC have been published aiming either at an increased activity, enantioselectivity or stability of the enzyme.[34–37] In contrast, HheG is rather thermolabile and much less selective. However, this HHDH was the first reported enzyme with relevant ring-opening activity towards sterically more demanding internal epoxides (cyclic as well as acyclic).[19,20,26–28,38] Even though less protein engineering data are available for HheG so far, the enzyme exhibits distinct structural differences compared to HheC.[20,26,27,38,39] This includes a much broader and open active site, an additional α-helix in the nucleophile binding site loop, as well as a long and highly flexible loop in the *N*-terminal part of the protein, modulating substrate access to but possibly also substrate binding in the active site.[20,40]

In this work, we experimentally examined all possible single mutants of HheC and HheG with defined amino acid exchanges at the three conserved motif 1 residues, namely threonine, phenylalanine/tyrosine and glycine (Figure 1A), to investigate the impact of each residue on enzyme activity, selectivity and stability. In this regard, our in-depth characterization revealed HheC F12Y to be enhanced considerably and towards multiple parameters. Complementary molecular dynamics (MD) and quantum mechanics (QM) simulations highlighted the formation of additional hydrogen bonds in mutant F12Y compared to HheC wild type, resulting in a better preorganization of the active site and a lower activation barrier for the epoxide ring-opening reaction. In addition, a

quantitative workflow for spectrophotometric activity determination in epoxide ring opening reactions has been developed, enabling also fast and reliable kinetic measurements.

RESULTS AND DISCUSSION

Mutagenesis and activity screening

To study the impact of motif 1 mutations on the activity, selectivity and stability of HHDHs, each of the three conserved residues of this motif (**T**-X_4-**F/Y**-X-**G**) in HheC and HheG was individually replaced by the corresponding other 19 proteinogenic amino acids using either a Golden Gate-based or MEGAWHOP mutagenesis strategy.[41,42] This resulted in a total of 112 defined single mutants, of which all could be generated successfully, except for mutants F12M and F12R of HheC. Subsequent heterologous production of all 110 mutants in *E. coli* BL21(DE3) in 15 mL scale and partial purification via *N*-terminal His-tag using gravity flow revealed that only few variants per position, usually carrying exchanges to structurally similar amino acids, still yielded observable amounts of soluble HHDH (Figure 1B and Figure S1). Hence, this result suggests a possible direct impact of motif 1 residues on protein folding and stability. As an exception, position F12 of HheC permitted more diverse mutations as almost all variants could be obtained as soluble proteins (Figure 1B and Figure S1).

Next, all generated mutants were screened for their dehalogenation and epoxide ring-opening activity in 96-well format. To this end, well-established model substrates for both the dehalogenation (dichloropropanol **1f** for HheC and chlorocyclohexanol **2f** for HheG) and the ring-opening reaction (epichlorohydrin **1** for HheC and cyclohexene oxide **2** for HheG) were used. For fast activity screening, we employed pH-based assays which have previously been reported in literature and make use of either phenol red or bromothymol blue as pH-indicators to detect qualitatively the amount of released (dehalogenation) or consumed free protons (epoxide ring opening) during catalysis (Figure S2 and Table S2).[43,44] For the exchange of the threonine (T7 in HheC and T13 in HheG) and glycine (G14 in HheC and G20 in HheG) in both enzymes only mutants carrying a chemically similar amino acid (serine instead of threonine, alanine instead of glycine) still exhibited detectable activity. In contrast, F12 in HheC displayed a much higher variability (Figure 1C) with HheC mutants F12G, F12A, F12C, F12S, F12Q, F12H, and F12Y being active in both dehalogenation and epoxide ring opening reactions. Interestingly, this was not the case for position Y18 of HheG. Here, only the exchange of tyrosine by phenylalanine yielded a mutant with significant activity. Those activity data are in full agreement with our results regarding the soluble expression of the generated mutants, with the only exception that not all soluble HheC F12X mutants were indeed also active. For all further tests, active HheC and HheG mutants of motif 1 were produced in larger scale and applied as FPLC-purified proteins (for yields see Table S1).

It should be noted here that Tian *et al.* do report a few active HheG mutants with amino acid exchanges at position Y18 of motif 1, which they obtained during protein engineering of this enzyme with the aim to improve enantioselectivity.[39] In their case, however, only whole-cell reactions have been performed, while we have been working with isolated enzymes instead. Thus, it is possible that those HheG mutants exhibit even more reduced stability or yield much less soluble enzyme compared to wild-type HheG, which is why we could have lost them during enzyme isolation and/or purification in our study. At the same time, this would reinforce our assumption that position 18 in HheG impacts protein folding and stability.

To facilitate more detailed kinetic analyses of the epoxide ring-opening reactions catalyzed by HHDHs in high throughput, we developed a quantitative pH indicator assay inspired by work from Gul and colleagues.[43] This assay relies on the conversion of a strong acid (e.g. azide) to a weak acid (e.g. an alcoholate) during epoxide ring opening, which increases the net pH value of the reaction mixture while the reaction progresses. Using bromothymol blue (**BTB**, an indicator with sweeping absorption spectra giving light yellow to dark blue mixtures) and dilute MOPS-buffered reaction mixtures, we typically followed ring-opening reactions starting at around pH 7. Unlike previously described assays using pH indicators,[43,44] our system returns quantitative conversion data by employing isometric normalization.[45–47] Using the isosbestic point of the deprotonation of **BTB**, we traced the deprotonation equilibrium of the indicator back to a concentration of consumed protons via the buffer strength (see the SI for details and mathematic operations). This assay proved readily compatible with high-throughput experimentation in 96-well plates and allowed straightforward monitoring of more than 20 reactions in parallel. Although we primarily used the assay for HHDH-catalyzed epoxide ring-opening reactions in our study, we expect it to be applicable to other proton-consuming or -liberating (biocatalytic) reactions as well.

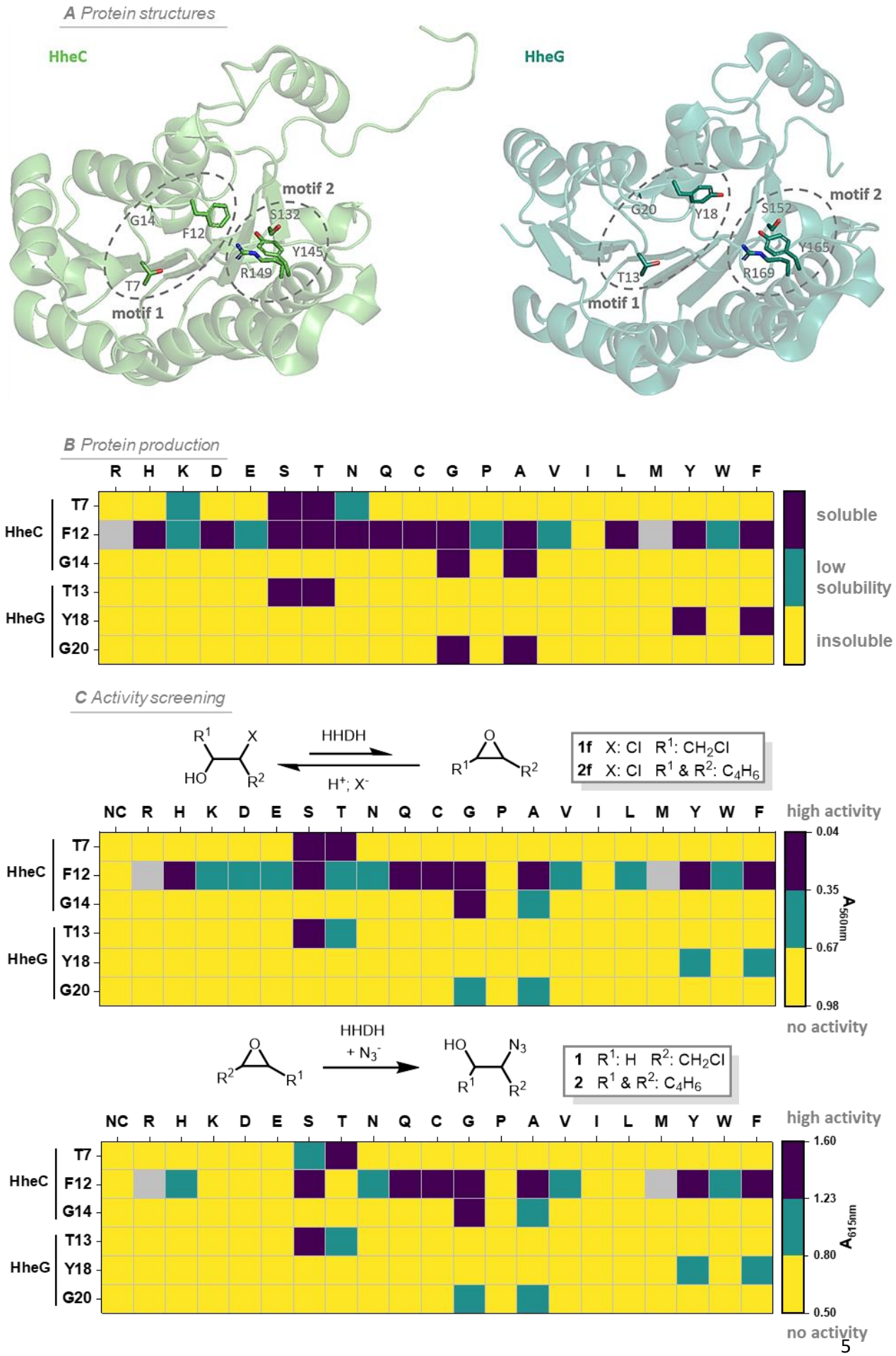

Figure 1. Summary of protein production and qualitative activity screening of motif 1 mutants of HheC and HheG. **A**) Crystal structures of HheC (green; PDB: 1PWX) and HheG (blue; PDB: 5O30) wild type with conserved residues of sequence motifs 1 and 2 highlighted. **B**) Solubility data of motif 1 mutants of HheC and HheG according to SDS-PAGE analysis (Figure S1). **C**) Activity screening data (dehalogenation and epoxide ring opening) of motif 1 mutants of HheC and HheG using qualitative pH indicator-based assays. High activity or solubility is represented by purple color, whereas no activity or insolubility is represented by yellow color. Grey color represents HheC mutants that could not be generated on genetic level.

Activity, stability and enantioselectivity of active mutants

Following the initial qualitative activity screen, we studied the epoxide ring-opening activity of active mutants with azide and various epoxides in more detail to gain further insights into the kinetic implications of motif 1 mutations on a broader range of substrates. Specifically, we used structurally diverse epoxides to cover relevant chemical space by employing epichlorohydrin (**1**), cyclohexene oxide (**2**), styrene oxide (**3**), phenyl glycidyl ether (**4**), limonene oxide (**5**), and *trans*-1-phenylpropylene oxide (**6**) (Figure 2A) and followed their conversion with our quantitative **BTB**-based pH assay. This analysis revealed that the introduction of mutations in motif 1 significantly impacted overall enzymatic activity (Figure 2B), even though the substrate spectra of the HheC and HheG mutants did not change compared to the wild type. Indeed, most mutants exhibited considerable reductions of their specific activities with all model substrates compared to the respective wild-type enzyme. The only variant in this panel which gained significant activity was HheC mutant F12Y, displaying a 3- to 5-fold increase in specific activity with **1** and **3**. Otherwise, even very conservative mutations, as for instance HheC mutant G14A and HheG mutant G20A, resulted in drastic losses of activity. This observation is in general agreement with the report of Jörnvall *et al.* on the mutagenesis of the corresponding conserved glycine residue in motif 1 of an SDR enzyme. Replacement of this glycine by alanine resulted in a 69% decrease in activity, while mutations G14V and G14N yielded almost inactive enzymes.[48]

The activity trends observed for the epoxide ring-opening direction generally carried over to the dehalogenation catalyzed by the motif 1 mutants. We examined this with the haloalcohols 1,3-dichloro-2-propanol (**1f**), 2-chlorocyclohexanol (**2f**) and 1,3-dibromo-2-propanol (**7g**) (Figure 2A), whose conversion could be followed discontinuously with a previously reported halide release assay.[49] While the specific activities of nearly all mutants were significantly reduced compared to the wild-type enzymes, HheC F12Y displayed considerably increased activity with the haloalcohols **1f** and **7g** (Figure 2C), mirroring the trends observed for the ring-opening activities. A higher activity of HheC mutant F12Y in the dehalogenation of 1,3-dichloro-2-propanol (**1f**) has previously been observed during thermostabilization of HheC by directed evolution.[24]

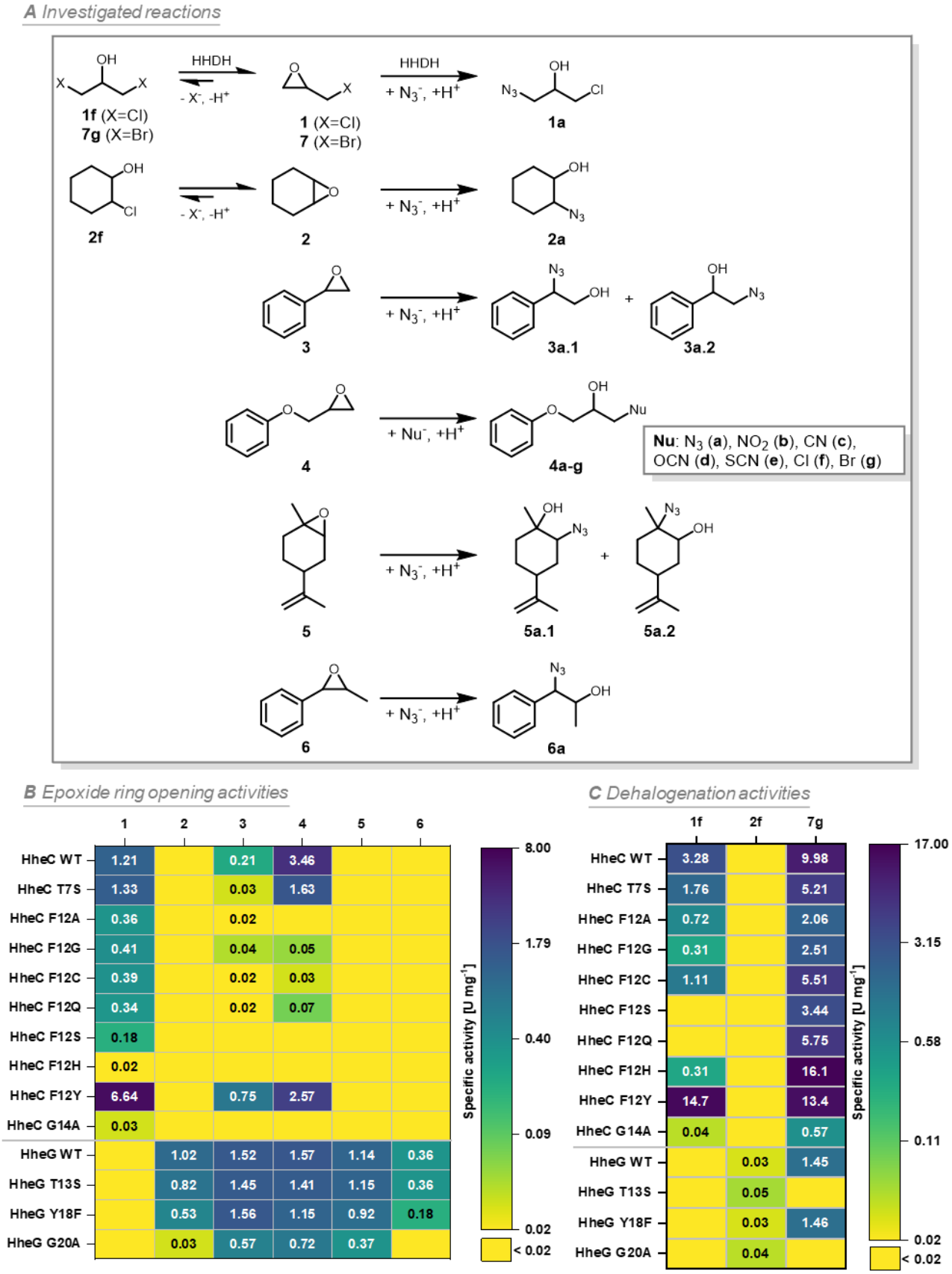

Figure 2. Specific activities (U mg^{-1}) based on initial reaction rates of active motif 1 mutants of HheC and HheG in dehalogenation and epoxide ring opening reactions. **A**) Overview of dehalogenation and epoxide ring opening reactions investigated in this study. **B**) Specific activities of HheC and HheG mutants as well as wild-type enzymes in epoxide ring opening reactions of epichlorohydrin (**1**), cyclohexene oxide (**2**), styrene oxide (**3**), glycidyl phenyl ether (**4**), (+)-*cis/trans*-limonene oxide (**5**) and *trans*-1-phenylpropylene oxide (**6**) determined via **BTB**-assay.

Reactions were performed in duplicate in a total volume of 1 mL with 10 mM epoxide and 20 mM azide in 2 mM MOPS buffer, pH 7.0 at 30 °C (HheC) or 22 °C (HheG) using 20−400 µg mL^{-1} purified enzyme (Table S3). Samples were taken after 30, 60, 180, 270 and 360 s. Chemical background of negative control reactions without enzyme addition was subtracted. The resulting specific activities exhibit standard deviations between 0.00 and 0.13 U mg^{-1}. **C**) Specific activities of HheC and HheG mutants as well as wild-type enzymes in the dehalogenation of haloalcohols 1,3-dichloro-2-propanol (**1f**), 2-chlorocyclohexanol (**2f**) and 1,3-dibromo-2-propanol (**7g**) determined via halide release assay. Reactions were carried out in duplicate in a total volume of 1 mL with 10 mM haloalcohol in 25 mM Tris·SO_4 buffer, pH 7.0 at 30 °C (HheC) or 22 °C (HheG) using 10−400 µg mL^{-1} purified enzyme (Table S4). Samples were taken after 30, 60, 180, 270, and 360 s. Chemical background of negative control reactions without enzyme addition was subtracted. The resulting specific activities exhibit standard deviations between 0.00 and 0.21 U mg^{-1}.

To unveil if the observed activity increase of HheC mutant F12Y is induced by an improved substrate binding or rather a significantly elevated reaction rate, we measured kinetic data for the dehalogenation of haloalcohol **1f** and the ring opening of epoxide **1** with azide using the halide release assay[49] as well as our **BTB**-based pH assay, respectively. Interestingly, this kinetic analysis revealed that the F12Y mutation only slightly impacted K_M or K_{50} for the substrates **1f** and **1** (Table 2). In contrast, the maximal reaction rates were considerably increased – 3.5-fold for the dehalogenation of **1f** and at least 5-fold in the azidolysis of **1** (rate improvement varies when either the kinetics for epoxide or azide are considered). Thus, the improved performance of HheC F12Y in dehalogenation and epoxide ring opening is solely caused by an enhancement of reaction velocities. For comparison, the corresponding K_{50} values of HheC mutants T7S and G14A for binding of epoxide **1** were increased by a factor of 2 or more compared to the wild type and mutant F12Y, indicating a lower substrate affinity of those motif 1 mutants in HheC. Moreover, HheC T7S exhibited an at least two-fold higher $k_{obs,max}$ compared to wild type, while the respective $k_{obs,max}$ of HheC G14A in the azidolysis of **1** was drastically reduced, both in line with our determined specific activities. Unfortunately, true k_{cat} values could not be determined in this epoxide ring opening reaction due to the high K_{50} values of all HheC mutants towards azide and the strong chemical background azidolysis of **1** occurring at azide concentrations above 100 mM. Therefore, kinetic measurements with varied epoxide concentration were performed at non-saturating azide concentration, yielding significantly lower $k_{obs,max}$ values compared to kinetic measurements with fixed epoxide and varying azide concentrations (Table 2). Importantly, all three HheC mutants do also exhibit higher K_{50} values as well as a considerably stronger cooperativity in azide binding – based on higher Hill coefficients n_H – than the corresponding wild-type enzyme (Table 2). Thus, those conserved residues in sequence motif 1 of HheC are indeed influencing nucleophile binding to a great extent. In contrast, changes in the kinetic parameters of HheG mutants compared to wild type in the azidolysis of epoxide **3** are less dramatic (Table 3), which is again in agreement with respective specific activities of HheG mutants determined for this reaction. The observed cooperativity for azide binding, however, again varies significantly depending on the introduced mutation.

Table 2. Kinetic parameters of selected HheC mutants in the dehalogenation of 1,3-dichloro-2-propanol (**1f**) (determined by halide release assay) as well as the azidolysis of epichlorohydrin (**1**) (determined by our **BTB** assay). For the latter reaction, first the epoxide concentration was varied while keeping the azide concentration constant at 100 mM; afterwards the azide concentration was varied fixing the epoxide concentration at 100 mM. The Michaelis-Menten equation was used to fit the resulting data for the dehalogenation of **1f**, whereas the Hill equation was used for fitting the experimental data obtained for the ring opening of **1** with azide.

	Kinetic parameters		HheC			
			WT	**T7S**	**F12Y**	**G14A**
1f	K_M	[mM]	0.45 ± 0.14	0.81 ± 0.23	0.98 ± 0.19	0.92 ± 0.37
	k_{cat}	[s^{-1}]	1.84 ± 0.11	1.37 ± 0.07	6.30 ± 0.26	0.05 ± 0.00
	k_{cat}/K_M	[mM^{-1} s^{-1}]	4.11 ± 1.33	1.70 ± 0.48	6.43 ± 1.33	0.06 ± 0.02
1	K_{50}	[mM]	18.8 ± 1.24	40.3 ± 6.88	14.2 ± 0.67	49.5 ± 1.52
	$k_{obs,max}$	[s^{-1}]	8.16 ± 0.25	25.4 ± 1.90	60.2 ± 1.18	0.78 ± 0.03
	$k_{obs,max}/K_{50}$	[mM^{-1} s^{-1}]	0.44 ± 0.03	0.63 ± 0.12	4.24 ± 0.22	0.02 ± 0.00
	n_H		1.70 ± 0.14	1.14 ± 0.10	2.32 ± 0.21	4.58 ± 0.79
Azide	K_{50}	[mM]	17.3 ± 2.29	80.9 ± 8.13	49.6 ± 2.49	111 ± 5.55
	$k_{obs,\ max}$	[s^{-1}]	27.0 ± 1.32	71.3 ± 4.72	137 ± 4.58	1.78 ± 0.08
	$k_{obs,max}/K_{50}$	[mM^{-1} s^{-1}]	1.55 ± 0.22	0.88 ± 0.11	2.76 ± 0.17	0.02 ± 0.00
	n_H		1.61 ± 0.26	3.28 ± 0.64	2.44 ± 0.27	3.59 ± 0.57

Table 3. Kinetic parameters of HheG mutants in the ring opening of cyclohexene oxide (**2**) with azide. The epoxide concentration was varied while keeping the azide concentration constant at 100 mM; afterwards the azide concentration was varied fixing the epoxide concentration at 100 mM. The Hill equation was used to fit the obtained experimental data.

Kinetic parameters			HheG			
			WT	T13S	Y18F	G20A
2	K_{50}	[mM]	39.4 ± 2.69	44.8 ± 1.29	66.4 ± 1.42	42.2 ± 3.64
	$k_{obs,max}$	[s^{-1}]	2.31 ± 0.15	3.34 ± 0.07	2.82 ± 0.06	1.02 ± 0.09
	$k_{obs,max}/K_{50}$	[mM^{-1} s^{-1}]	0.06 ± 0.01	0.07 ± 0.01	0.04 ± 0.00	0.02 ± 0.01
	n_H		3.81 ± 0.78	3.67 ± 0.33	3.96 ± 0.25	3.28 ± 0.63
Azide	K_{50}	[mM]	38.4 ± 2.08	24.0 ± 1.59	26.4 ± 3.73	33.7 ± 0.57
	$k_{obs,max}$	[s^{-1}]	4.12 ± 0.15	5.31 ± 0.17	2.77 ± 0.17	1.74 ± 0.18
	$k_{obs,max}/K_{50}$	[mM^{-1} s^{-1}]	0.11 ± 0.01	0.22 ± 0.02	0.11 ± 0.02	0.05 ± 0.00
	n_H		2.92 ± 0.36	2.40 ± 0.28	1.74 ± 0.27	3.90 ± 0.23

Next, we probed the enantioselectivity of our motif 1 mutants in epoxide ring opening reactions with azide to test if motif 1 mutations affected also the selectivity of these enzymes. For variants of HheC, we selected the terminal epoxides **1** and **3** as substrates, while we used **3** and the cyclic epoxide **2** for HheG variants. Our choice of epoxide **3** was primarily motivated by the opposite regioselectivity of HheC and HheG in their ring opening of this substrate (Figure S3).[8] The non-catalyzed reaction preferentially yields 2-azido-2-phenylethan-1-ol (**3a.1**) through nucleophilic attack at the benzylic α-carbon. While HheG enforces this inherent preference, HheC exhibits selectivity for attack at the terminal β-position. Biotransformations analyzed by chiral GC revealed that most of the motif 1 mutations in HheC decreased enantioselectivity significantly compared to the wild-type enzyme, independently of the epoxide substrate (Table 4). In contrast, mutants T7S and F12Y displayed a greatly increased enantioselectivity in the conversion of **1** with azide, while the extremely high enantioselectivity of the wild type enzyme with **7** was maintained. This indicates a considerable impact of motif 1 residues on the enantioselectivity of HheC. On the other hand, the enantioselectivity of the studied HheG mutants in the ring opening of **2** and **3** hardly changed compared to HheG wild type (Table 4). For comparison, mutations at the central aromatic residue Y18 in the homologous HheG enzyme from *Acidimicrobiia* bacterium did affect enantioselectivity in the ring opening of **3** with cyanate.[14] Apart from this overall varying influence of motif 1 residues on enantioselectivity, all herein studied HheC and HheG mutants retained the wild-type enantiopreference for the conversion of (*S*)-**1** and (*R*)-**3**.

Following these activity and enantioselectivity studies, we also examined the thermal stability of active motif 1 mutants of HheC and HheG by differential scanning fluorimetry (also known as thermofluor assay), as a positive impact of mutation F12Y on the thermostability of HheC has previously been reported.[24] Our analysis revealed a considerable stabilizing effect for mutations F12H (+10.5 K), F12Y (+10.1 K) and G14A (+7.3 K) in HheC (Figure S4). The latter is especially surprising as this mutation heavily decreased enzyme activity. In contrast, the opposite trend in thermal stability has previously been reported for the exchange of the equivalent glycine residue in SDR motif 1 of *Drosophila* alcohol dehydrogenase,[50] and was also observed in our study for the corresponding mutation G20A in HheG. The herein reported stabilizing effect of mutation F12Y in HheC was previously attributed to the formation of an additional hydrogen bond with residue T131 compared to wild-type HheC, which we could confirm based on our computational results (see below).[24] A slight increase (+2.8 K) in the apparent melting temperature of HheG upon exchange of the corresponding tyrosine 18 by phenylalanine becomes apparent from Figure S4 as well.

Table 4. Enantioselectivity of HheC mutants and wild type (WT) in the azidolysis of 10 mM epichlorohydrin (**1**) and styrene oxide (**3**), as well as enantioselectivity of HheG mutants and wild type (WT) in the azidolysis of 10 mM cyclohexene oxide (**2**) and styrene oxide (**3**). "C" represents conversion and "NC" represents negative control reactions without enzyme addition.

HheC[a]									
	Epoxide 1				Epoxide 3				
Mutant	**Enzyme conc. [µg mL^{-1}]**	**C [%]**	**ee$_P$ [%]**	**E**	**Enzyme conc. [µg mL^{-1}]**	**C$_\beta$[b] [%]**	**ee$_S$ [%]**	**ee$_{P\beta}$ [%]**	**E$_\beta$[b]**
NC	-	5.0	0.1	-	-	0.0[c]	0.0	-	-
WT	10	46.5	82.6	22 (*S*)	25	29.1	35.4	99.9	>200 (*R*)
T7S	10	33.6	94.5	57 (*S*)	25	29.4	37.2	99.9	>200 (*R*)
F12A	400	50.9	62.5	8.3 (*S*)	400	28.4	72.8	36.7	2.5 (*R*)
F12G	400	51.1	45.5	4.2 (*S*)	400	19.5	73.2	39.1	2.5 (*R*)
F12S	400	20.8	46.2	3.1 (*S*)	400	20.4	73.2	25.9	1.8 (*R*)
F12C	400	40.4	64.5	7.0 (*S*)	400	16.9	0.83	45.3	2.9 (*R*)
F12Q	400	52.4	51.0	5.3 (*S*)	400	12.2	0.50	47.6	3.0 (*R*)
F12H	400	28.5	81.7	17 (*S*)	400	21.8	73.9	26.2	1.8 (*R*)
F12Y	10	45.3	93.8	74 (*S*)	25	34.5	44.7	99.9	>200 (*R*)
G14A	400	5.34	16.4	1.4 (*S*)	400	12.0	12.8	93.9	36.2 (*R*)

HheG[a]								
	Epoxide 2			Epoxide 3				
Mutant	**Enzyme conc. [µg mL^{-1}]**	**C [%]**	**ee$_P$ [%]**	**Enzyme conc. [µg mL^{-1}]**	**C$_\alpha$[d] [%]**	**ee$_S$ [%]**	**ee$_{P\alpha}$ [%]**	**E$_\alpha$[d]**
NC	-	0.1	0.1	-	5.6	0.1	0.1	-
WT	100	60.8	48.1 (*S*)	50	53.9	88.8	76.1	22 (*S*)
T13S	100	75.4	46.2 (*S*)	50	49.5	74.7	76.4	17 (*S*)
Y18F	100	53.6	56.1 (*S*)	50	48.6	72.4	76.5	16 (*S*)
G20A	400	23.6	50.6 (*S*)	400	43.3	32.1	42.2	3.3 (*S*)

[a] Reactions were carried out in a total volume of 1 mL in 50 mM Tris·SO_4, pH 7.0, at 30 °C (HheC) or 22 °C (HheG) and 900 rpm using 10-400 µg mL^{-1} purified enzyme. Samples were taken after 15 min (epoxide **1**) or 1 h (epoxide **3**), extracted with an equal volume of *tert*-butyl methyl ether and analyzed by achiral and chiral GC.

[b] Conversion and enantioselectivity towards formation of product 2-azido-1-phenylethan-1-ol (**3a.2**) through nucleophilic attack at the terminal β-position.

[c] In the non-catalyzed chemical background reaction, formation of product 2-azido-2-phenylethan-1-ol (**3a.1**) through nucleophilic attack at the benzylic α-carbon is preferred.

[d] Conversion and enantioselectivity towards formation of product 2-azido-2-phenylethan-1-ol (**3a.1**) through nucleophilic attack at the benzylic α-carbon.

Taking into account that HheC mutant F12Y is not only more active in the dehalogenation and epoxide ring opening of several tested substrates, but exhibits also higher enantioselectivity and thermal stability compared to wild-type HheC, the question arises why mutation F12Y was not selected during natural evolution of this enzyme. For comparison, other native HHDHs such as HheB or HheG carry a tyrosine instead of a phenylalanine at the respective motif 1 position. One possible hypothesis might be that mutant F12Y is not superior in combination with HheC's natural substrate(s), as the epoxides and haloalcohols tested by us probably do not represent natural substrates of HheC. In agreement with this hypothesis, mutant F12Y is not generally more active independent of the used substrate, but was found to display a lower specific activity in the azidolysis of glycidyl phenyl ether. On the other hand, the gene of HheC is organized in an operon together with an epoxide hydrolase-encoding gene in the genome of *A. radiobacter*. Both enzymes were predicted to act together in the detoxification of harmful haloalcohols.[15] Thus, HheC's activity in *A. radiobacter* likely needs to be harmonized with the respective activity of the epoxide hydrolase to prevent an accumulation of the epoxide intermediate, which is harmful itself due to its high reactivity with e.g. primary amines of lysine residues. A too high activity of HheC might therefore not be evolutionary beneficial.

Nucleophile acceptance of active motif 1 mutants

Since amino acids of sequence motif 1 line the nucleophile-binding pocket of HHDHs, we also expected a possible impact of those residues on nucleophile binding, as already observed for the nucleophile azide during our kinetic studies of motif 1 mutants. Thus, we further focused on a potential change in nucleophile acceptance after mutagenesis of motif 1 residues using a broader range of nucleophiles. In this regard, mutants T7S, F12Y and G14A of HheC as well as HheG mutants T13S, Y18F and G20A were applied in epoxide ring opening reactions of phenyl glycidyl ether (**4**) using azide, nitrite, cyanide, cyanate, thiocyanate as well as the halides chloride and bromide as nucleophiles. Those nucleophiles have previously been demonstrated to be accepted by HheC and HheG wild type.[10,28] To cover an activity range as large as possible, conversions of enzyme-catalyzed transformations were determined after short (1 h) but also extended (24 h) reaction times (Figure 4A). These experiments revealed that the overall nucleophile acceptance of HheC and HheG was not altered considerably upon mutagenesis. However, a few interesting results stand out. For instance, HheG mutant G20A displayed surprisingly high activity with the nucleophiles thiocyanate and bromide, almost in the range of wild-type HheG, while it was virtually inactive with all other tested nucleophiles. However, the same effect was not noticed for HheC G14A, which might be related to the overall much lower activity of HheC with thiocyanate. As reported earlier[28], epoxide ring opening with thiocyanate can occur via *S*- and *N*-nucleophilic attack yielding two different product isomers, which were also observed in our study. Their ratio, however, did not change depending on the applied enzyme variant (Figure 4B). In contrast, the ratio of formed diol and nitroalcohol product in the ring opening of **4** with nitrite as nucleophile indeed varied to some extent depending on the respective motif 1 mutation. In this case, the diol product occurs due to *O*-nucleophilic attack at the epoxide and subsequent hydrolysis of the formed nitrite ester. Interestingly, especially the preference of HheC mutant T7S and HheG mutant G20A for diol formation was increased in comparison to respective wild-type enzymes (Figure 4B). Those results again underscore the impact of motif 1 residues on nucleophile binding and selectivity.

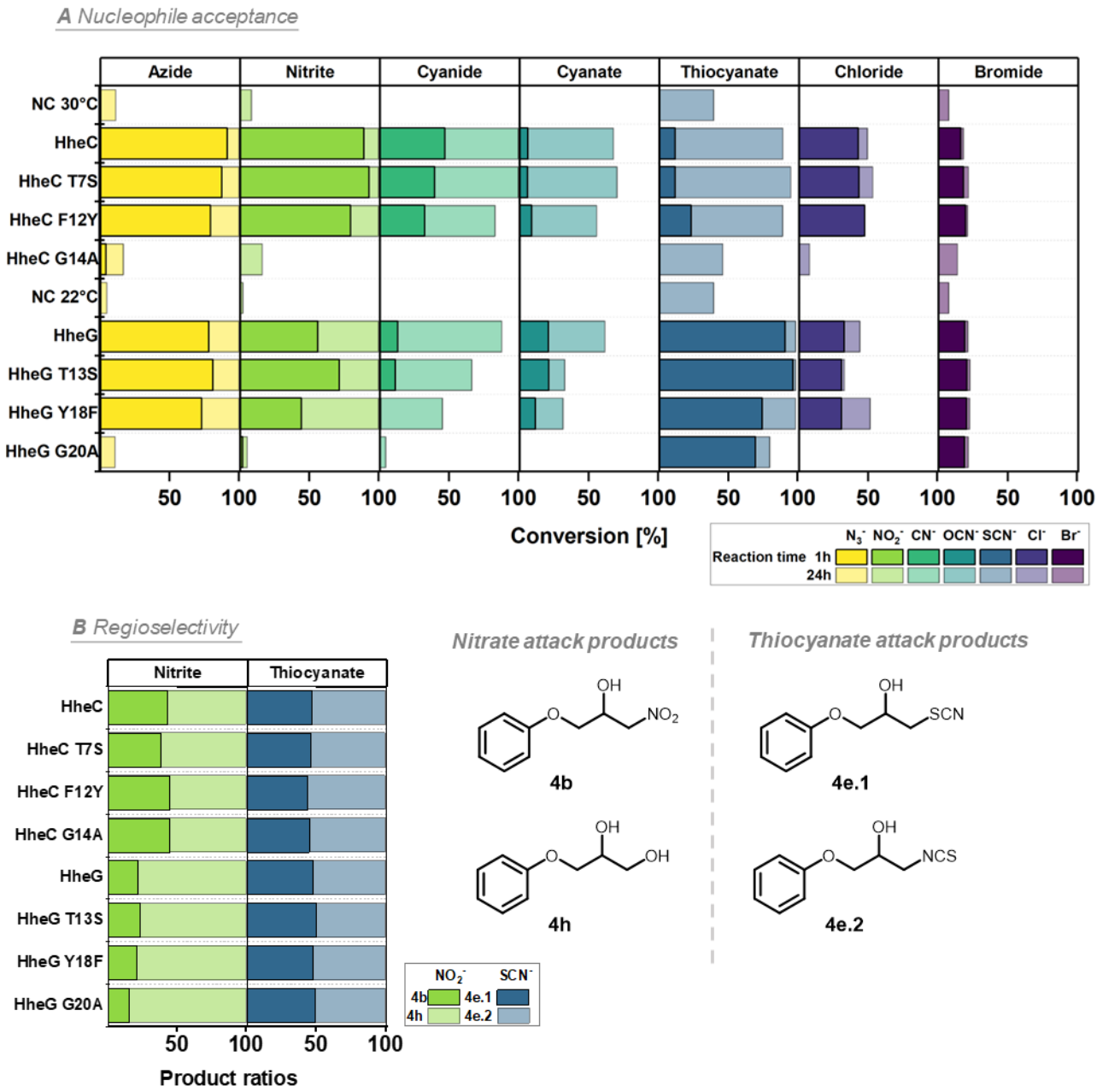

Figure 4. Nucleophile acceptance of motif 1 mutants. **A)** Conversions of 10 mM glycidyl phenyl ether (**4**) with 20 mM nucleophile (azide, nitrite, cyanide, cyanate, thiocyanate, chloride, bromide) in 50 mM Tris·SO_4 buffer, pH 7.0, at 30 °C (HheC) or 22 °C (HheG) and 900 rpm using each 150 µg mL^{-1} purified enzyme. Reactions were carried out in a total volume of 1 mL. Samples were taken after 1 h and 24 h, extracted with an equal volume of *tert*-butyl methyl ether and analyzed by achiral GC. "NC" represents negative control reactions without enzyme addition. **B)** Ratio of formed products in reactions with nucleophiles nitrite and thiocyanate.

Computational analyses

Intrigued by how the central aromatic residue in motif 1 enhances HheC activity towards the epoxide-ring opening reaction, we decided to computationally evaluate HheC wild-type and mutant F12Y by means of Quantum Mechanics (QM) and Molecular Dynamics (MD) simulations. Considering the proximity of position F12 to the catalytic residues (Figure 5A) and the big impact on reaction rate (Table 2), we hypothesized that the additional hydroxyl group could potentially establish hydrogen bonds with either the catalytic and binding residues, the nucleophile binding pocket and/or the substrates epichlorohydrin (**1**) and azide to promote catalysis. To elucidate whether mutation F12Y directly impacts the activation barrier for the epoxide ring-opening reaction, we generated a cluster model of the active site and used DFT as done previously by the group of Himo (Figure 5A, 5B).[21]

We observed that both in the reactant complex (**RC**) (Figure S10) and the transition state (**TS1**) the additional hydroxyl group thanks to mutation F12Y can establish a hydrogen bond with azide, which helps to retain the

nucleophile in the nucleophile binding pocket and more importantly positions azide in a good orientation for epoxide-ring opening (Figure 5A, left panel). The terminal nitrogen of azide establishes a hydrogen bond with the backbone of L178 and the hydroxyl group of Y12, whereas the nitrogen involved in the nucleophilic attack is hydrogen-bonded to a crystallographic water molecule (Figure 5A, left panel). This hydrogen bond network impacts the charge distribution at the azide and favors the accumulation of more negative partial charge at the nitrogen responsible for the nucleophilic attack (Table S5). The activation barrier at this conformation towards the epoxide ring opening of **1** is *ca.* 9 kcal/mol at the M06-2X/Def2-TZVPP level of theory. We located another **TS2** that does not present the F12Y-azide interaction, instead the terminal nitrogen of azide makes a hydrogen bond with both the crystallographic water molecule and L178 (Figure 5A, right panel). This difference in the hydrogen bond network with respect to **TS1** slightly modifies the negative charge on the nucleophilic nitrogen of the azide, thus leading to an activation barrier for **TS2** *ca.* 6 kcal/mol higher than for **TS1** (the activation barrier for **TS2** is ca. 16 kcal/mol). This additional **TS2** is extremely similar to the one found for HheC wild type (Figure 5B). In the wild type, the activation barrier for the ring opening of **1** is *ca.* 14 kcal/mol as found for **TS2** in the case of F12Y. The computed barriers are in line with the previously reported barriers for HheC with azide and other epoxides reported by Himo and coworkers.[21] It should be mentioned that the large differences in the activation barriers found for HheC F12Y and wild type are overestimated as compared to the experimental kinetic constants, but in line with the observed big impact of mutation F12Y on the catalytic turnover (minimum 5-fold increase in $k_{obs,max}$). We observed in the DFT-optimized **RC** as well as **TS2** that F12Y makes a hydrogen bond with the carbonyl backbone of P175 (the distance between the hydrogen of the hydroxyl group of Y12 and the oxygen of the backbone of P175 is *ca.* 2 Å in all cases, see Figure S10 and 5A). The carbonyl group of P175 was found to provide electrostatic stabilization to C_β, which favors the attack at this position.[21] The hydrogen bond established between the hydroxyl group of F12Y and P175 induces a slight bend of the carbonyl backbone. HheC mutant F12Y therefore also favors the proper positioning of the P175 backbone close to the epoxide substrate and favors the attack at the less substituted carbon.

We hypothesized that mutation F12Y could also help in the preorganization of the active site pocket, thus impacting and favoring the productive binding of the azide (and epoxide) in place for the ring-opening reaction to occur. To that end, we ran nanosecond timescale MD simulations for both HheC wild type and mutant F12Y in the absence of any substrate, and in the presence of epoxide **1** and azide in the active site. The analysis of the MD simulations in the absence of any ligand indicated that F12Y establishes a hydrogen bond with the backbone of T131 that is adjacent to the catalytic S132 (Figure 5C, 5D). This interaction established between the hydroxyl group of Y12 and T131, which is obviously not possible in HheC wild type, has some important implications for the active site preorganization. Thanks to this interaction, the loop containing F12Y is slightly more rigid (Figure 5C), which helps in retaining azide in place for the epoxide-ring opening reaction (Figure 5D, right panel). In HheC wild type, such an interaction is not possible, thus the side chain of F12 is substantially more flexible and clearly affects the binding of the azide in the nucleophile binding pocket (Figure 5D, left panel). Moreover, this newly established hydrogen bond between Y12 and T131, and the resulting loop rigidification likely contribute to the observed higher thermal stability of HheC mutant F12Y as well, as suggested previously.[24]
Although the kinetic constant ($k_{obs,max}$) for mutant F12Y is substantially improved, the mutation at the same time affects the binding of azide and induces stronger cooperativity (Table 2). The higher K_{50} value found for azide in mutant F12Y can be explained by the distance between azide and position F12Y (Figure S11). In F12Y, azide can adopt two different binding modes: the catalytically productive pose as shown in Figure 5D, and an additional one in which azide displaces the epoxide and interacts with both the catalytic S132 and F12Y. This additional, catalytically non-productive binding mode likely causes the higher K_{50} value found experimentally for azide in mutant F12Y (Table 2). We additionally applied our correlation-based tool Shortest Path Map (SPM)[51,52] to investigate how the communication network between subunits might be altered through mutation F12Y (Figure S12). Interestingly, we observed a much more interconnected network in mutant F12Y, thus suggesting that the establishment of the Y12-T131 interaction enhances the intramolecular interactions and the allosteric communication between subunits. This is in line with the higher Hill coefficient of HheC F12Y found experimentally (Table 2).

In summary, the QM and MD simulations of HheC wild type and F12Y in complex with epoxide **1** and azide indicate that mutation F12Y changes the network of hydrogen bonding with azide, which has a big impact on the activation barrier, but also on the preorganization of the active site and the retention of both epoxide and azide at their required optimal positions for enhanced activity. In comparison, the equivalent tyrosine 18 in HheG wild type is not able to establish similar hydrogen bonding interactions with azide or T151 (equivalent to T131 in HheC) due to the much wider active site pocket of HheG. The latter might explain why mutation Y18F in HheG affects enzyme activity only slightly (*vide infra*).

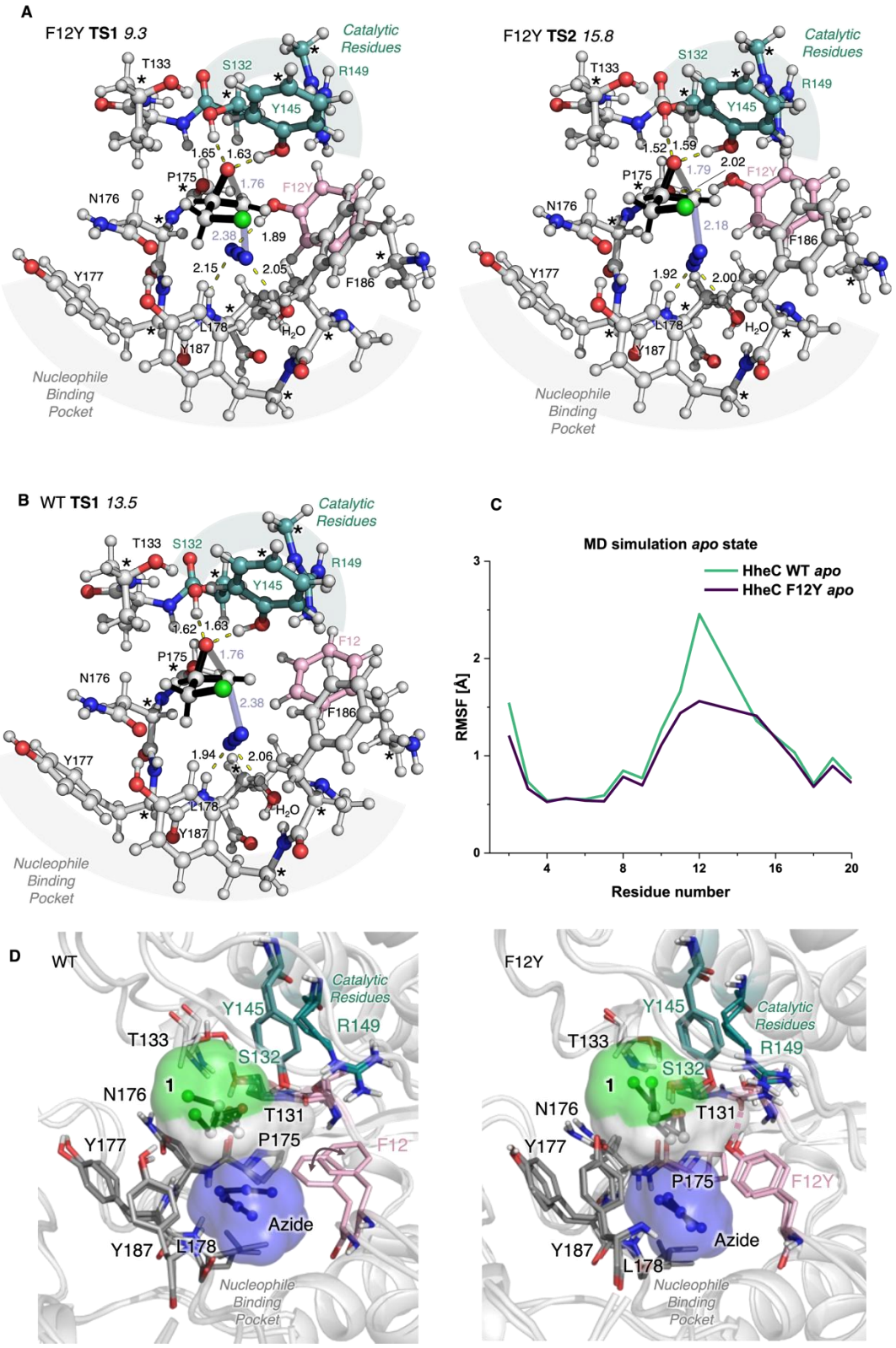

Figure 5. QM-optimized TS for the epoxide ring-opening reaction of **1** with azide for: (**A**) HheC variant F12Y (**TS1**, left and **TS2**, right panel) and **(B**) **TS1** for HheC wild type (WT). The computed activation energies are included in kcal/mol. All atoms restrained in the cluster model are marked with a star. **TS1** of WT and **TS2** of F12Y are very similar and present azide establishing hydrogen bonds with the terminal nitrogen and the backbone of L178 and a water molecule. In **TS1** of variant F12Y, the nitrogen of azide undergoing the nucleophilic attack is hydrogen bonded to the water molecule, and the terminal nitrogen to the backbone of L178 and the hydroxyl group of the F12Y mutation. (**C)** Root Mean Square Fluctuation (RMSF) computed considering the C_β atoms along the nanosecond timescale MD simulations in the absence of azide and epoxide. (**D**) Overlay of two representative conformations

extracted from the MD simulations performed with both epoxide **1** and azide for WT (left) and mutant F12Y (right). The extra flexibility of residue F12 in WT (highlighted with a double arrow) affects the productive binding of azide in the active site pocket, thus hampering the epoxide-ring opening reaction.

CONCLUSION

Overall, we have demonstrated that important enzyme properties of HHDHs, such as activity, selectivity and stability, are influenced by the conserved residues threonine, phenylalanine/tyrosine and glycine of sequence motif 1 (**T**-X_4-**F**/**Y**-X-**G**), which lines the nucleophile binding pocket of HHDHs. Despite the fact that those three residues appear to be highly conserved among naturally occurring HHDHs (please note that two highly homologous natural variants with sequence motif variation at the threonine position have been reported very recently[14,53]), we could show that especially the aromatic residue (phenylalanine/tyrosine) and the threonine position can be mutated to adjust enzyme properties, as exemplified for HheC. Only the conserved glycine residue of motif 1 proved quite invariable in both studied HHDHs as even the exchange by alanine resulted already in drastic activity losses toward most tested dehalogenation and epoxide ring opening reactions.

Even though the actual effect of individual mutations is mainly enzyme dependent, mutagenesis of motif 1 residues can yield greatly improved enzyme variants such as HheC F12Y. This mutant features not only a higher thermal stability as reported earlier[24], but displays also much higher activity in the dehalogenation and epoxide ring opening of most substrates tested herein, as well as an impressive enantioselectivity improvement in the ring opening of epichlorohydrin (**1**), making this variant highly attractive for biocatalytic applications. Moreover, the detailed molecular insights into the activity improvement induced by mutation F12Y, which have been gained through QM and MD simulations in this study, will facilitate further protein engineering campaigns of HheC starting from mutant F12Y in the future.

EXPERIMENTAL SECTION

Chemicals

Substrates epichlorohydrin, 1,3-dichloropropanol, 1,3-dibromopropanol, (*R*)-epichlorohydrin were purchased from Acros Organics (Geel, Belgium). Substrates cyclohexene oxide and styrene oxide were obtained from Thermo Fisher Scientific (Geel, Belgium). Substrates 2-chloro cyclohexane-1-ol, glycidyl phenyl ether, phenylpropylene oxide, limonene oxide and (*S*)-epichlorohydrin were purchased from Merck (Darmstadt, Germany). Nucleophiles sodium azide, sodium nitrite, potassium chloride, potassium bromide, potassium cyanate, sodium cyanide and sodium thiocyanate were purchased from Thermo Fisher Scientific (Geel, Belgium). (*R*)-styrene oxide was purchased from abcr (Karlsruhe, Germany). All chemicals were of highest available purity.

Bacterial strains and plasmids

Escherichia coli BL21(DE3) was used for heterologous protein production as outlined before.[19,20,26] All genes were expressed from vector pET-28a(+) (Merck) under control of the T7 promoter, resulting in the addition of an N-terminal hexahistidine (His_6)-tag to the heterologously produced proteins.[18]

HheC and HheG mutagenesis

Amino acid positions for mutagenesis were selected based on the respective motif 1 sequences of HheC (T-X_4-F-X-G) and HheG (T-X_4-Y-X-G). For each conserved amino acid position within motif 1, variants carrying all 19 possible amino acid exchanges were generated using site-directed mutagenesis (see Table S6 for a list of used primers). In case of positions T13, Y18 and G20 of HheG as well as T7 and G14 of HheC, a Golden Gate mutagenesis protocol was used (see supplementary Table S7 for details regarding the composition of the PCR reaction).[41] The PCR protocol for plasmid amplification while introducing the mutation consisted of an initial denaturation (98 °C, 30 s), 30 cycles of denaturation (98 °C, 10 s), annealing (T_m-5 °C, 30 s) and elongation (72 °C, 30 s kb^{-1}), followed by a final elongation step (72 °C, 120 s). After successful generation of mutated linear plasmids, one-pot restriction and ligation was performed using 1x cut smart® buffer (NEB), 1x T4-ligase buffer, 2 U BsaI, 400 U T4-ligase and 150 ng PCR product in 20 µL, and was incubated for 2 h at 30 °C, followed by heat inactivation of the reaction for 20 min at 65 °C. Resulting plasmids were transformed into *Escherichia coli* BL21(DE3) cells *via* heat shock method.[54,55] Correct insertion of desired mutations was confirmed by sequencing.

For position F12 of HheC, a MEGAWHOP mutagenesis protocol was used.[42] Respective MEGA-primers were generated using QuikChange® mutagenic reverse primers in combination with a T7 forward primer (Table S6). Reaction conditions (see Table S7) as well as the PCR protocol were the same as for Golden Gate mutagenesis except for the used annealing condition, which was set to 57 °C for 30 s. For the subsequent MEGAWHOP mutagenesis, 300 ng of purified MEGA-primer, 30 ng pET28a(+)-*hheC* and PfuUltra II Hotstart PCR Mastermix (Agilent Technologies, Santa-Clara, CA, United States) were applied. The PCR protocol consisted of an initial

denaturation step (98 °C, 30 s), 30 cycles of denaturation (98 °C, 10 s), annealing (55 °C, 30 s) and elongation (68 °C, 2 min kb^{-1}), followed by a final elongation step (72 °C, 120 s).

Protein production and purification

Small-scale production of all HheC and HheG mutants was performed in 50 mL reaction tubes in a total volume of 15 mL of Terrific Broth (TB) (per liter: 4 mL glycerol, 12 g peptone, 24 g yeast extract, 0.17 M KH_2PO_4, 0.74 M K_2HPO_4) supplemented with 50 µg mL^{-1} kanamycin and 0.2 mM isopropyl-β-D-thiogalactopyranosid (IPTG), and inoculated with 10% (v/v) preculture. After incubation for 24 h at 22 °C and 220 rpm, cells were harvested by centrifugation (20 min, 3488 *g*, 4 °C) and the resulting cell pellets were stored at -20 °C until further use. For small-scale purification via N-terminal His-tag, cell pellets were resuspended in 2 mL buffer A (50 mM Tris·SO_4, 300 mM Na_2SO_4, 25 mM imidazole, pH 7.9), supplemented with 1 mg mL^{-1} lysozyme and one Pierce Protease Inhibitor Mini Tablet (EDTA-free, Life Technologies, Thermo Fisher Scientific). Cells were disrupted by sonication on ice for 3 min (6 cycles of 10 s pulse and 20 s pause). Cell debris were removed by centrifugation (30 min, 21 000 *g*, 4 °C). The resulting cell-free extracts were loaded on 0.8 mL Pierce® centrifuge columns with a column volume (CV) of 0.6 mL Ni Sepharose™ 6 fast flow (GE Healthcare, Freiburg, Germany), pre-equilibrated with buffer A. After protein binding, columns were washed with each 10 CV of buffer A to remove non-specifically bound proteins. Elution of His_6-tagged target proteins was performed using 1.5 CV of buffer B (50 mM Tris·SO_4, 300 mM Na_2SO_4, 500 mM imidazole, pH 7.9) and fractions of each 1 mL were collected. For desalting, 1 mL elution fraction was loaded onto PD MidiTrap™ G-25 desalting columns (GE Healthcare), pre-equilibrated with TE buffer (10 mM Tris·SO_4, 4 mM EDTA, pH 7.9, 10% (v/v) glycerol), and eluted with 1.5 mL TE-buffer. Protein concentrations were determined based on absorbance at 280 nm using a NP80 nanophotometer (Implen, München, Germany) and respective molar extinction coefficients obtained by Protparam[56].

Selected active mutants of HheC and HheG as well as wild-type enzymes were produced in larger scale in shake flasks using the same protocol as mentioned above but 500 mL TB medium.[20] Cells were harvested by centrifugation (20 min, 3494 *g*, 4 °C) and resulting cell pellets were stored at −20 °C until further use. For purification via N-terminal His-tag, cell pellets were resuspended in 30 mL buffer A, supplemented with 1 mg mL^{-1} lysozyme and one Pierce Protease Inhibitor Mini Tablet, and disrupted by sonication on ice for 7 min (14 cycles of 10 s pulse and 20 s pause). Cell debris were removed by centrifugation (45 min, 18000 *g*, 4 °C) and resulting cell-free extracts were filtered through a 0.45 µm syringe filter. Cell-free extracts were loaded (2 mL min^{-1} flow rate) on a 5 mL HisTrap FF column (GE Healthcare, Freiburg, Germany), pre-equlibrated with buffer A, using an ÄktaStart FPLC system (GE Healthcare). Afterwards, the column was washed with 10 CV of buffer A to remove non-specifically bound proteins. His_6-tagged target protein was eluted using a gradient from 0 to 100% buffer B in 60 mL while collecting fractions of each 1 mL. Fractions with highest UV absorbance at 280 nm were combined and concentrated to a volume of 2.5 mL using Vivaspin Turbo 15 centrifugation units (Sartorius, Göttingen, Germany) with 10 kDa molecular weight cut-off. For desalting, the concentrated protein solutions were loaded onto PD10 desalting columns (GE Healthcare), pre-equilibrated with TE buffer, and eluted with 3.5 mL TE-buffer. Respective yields of purified HheC and HheG variants are listed in Table S1.

pH-indicator assays for initial qualitative activity screening

All mutants of HheC and HheG were screened with regard to their dehalogenation and epoxide ring opening activities using two different pH-indicator assays. Dehalogenation reactions contained 2 mM HEPES·SO_4 pH 8.2, 1 mM haloalcohol substrate (1,3-dichloropropanol (**1f**) or 2-chloro-1-cyclohexanol (**2f**) in case of HheC and HheG mutants, respectively), 20 µg mL^{-1} phenol red as well as 50 µg mL^{-1} purified enzyme in a total volume of 200 µL.[44] Reactions were performed in 96-well plates (Sarstedt, Nümbrecht, Germany) at 22 °C (HheG) or 30 °C (HheC) for 30 min with shaking at 500 rpm on incubating microplate shaker (VWR, Darmstadt, Germany). Subsequently, the absorbance of each well at 560 nm was measured using a ClarioStar microplate reader (BMG LABTECH GmbH, Ortenberg, Germany).

Epoxide ring opening activity was determined using bromothymol blue as pH-indicator.[43] Reactions contained 10 mM epoxide substrates (cyclohexene oxide (**2**) or epichlorohydrin (**1**) in case of HheG and HheC mutants, respectively), 20 mM azide, and 50 µg mL^{-1} purified enzyme in 2 mM MOPS·SO_4 pH 7.0 in a total volume of 180 µL. Reactions were performed in 96-well plates (Sarstedt, Nümbrecht, Germany) at 22 °C (HheG) or 30 °C (HheC) for 30 min with shaking at 500 rpm on on incubating microplate shaker (VWR, Darmstadt, Germany). Subsequently, bromothymol blue was added to a final concentration of 20 µg mL^{-1} and absorbance of each well at 615 nm was measured using a ClarioStar microplate reader (BMG LABTECH GmbH, Ortenberg, Germany).

Optimized bromothymol blue assay for quantitative analysis of epoxide ring opening

For determination of specific activities in epoxide ring opening with epoxide substrates **1**, **2**, **3**, **4**, **5**, and **6** using azide as nucleophile, reactions of 1 mL total volume contained 10 mM epoxide, 20 mM azide, and 10−400 µg mL^{-1} purified enzyme in 2 mM MOPS·SO_4 pH 7.0. Reactions were incubated at 22 °C (HheG wild type and mutants) or

30 °C (HheC wild type and mutants) with shaking at 900 rpm in a ThermoMixer C from Eppendorf (Hamburg, Germany). Samples of each 100 µL were taken after 30−360 s and transferred to a 96-well plate containing already 100 µL quenching solution (40 µg mL^{-1} BTB in 100% methanol) per well. Afterwards, absorbance at 616 nm and 499 nm was measured using a ClarioStar microplate reader. Activities were calculated using equations S8, 10, 15, 17, 18 in the supplementary.

This assay was also used for the determination of kinetic parameters in epoxide ring opening reactions. For kinetic measurement of HheC and its mutants, reactions were carried out in 2 mM MOPS·SO_4 using 1−150 mM epichlorohydrin (**1**) while keeping the azide concentration fixed (60 mM for HheC WT, T7S, F12Y, 100 mM for HheC G14A) or using 1-300 mM azide while keeping the concentration of epoxide **1** constant at 100 mM. Reactions were incubated at 30 °C. Samples were taken after 30-360 s to ensure determination of initial velocities. For HheG and its mutants, reactions were performed in 2 mM MOPS·SO_4 using 1-150 mM cyclohexene oxide (**2**) while keeping the azide concentration fixed (60 mM for HheG WT, T13S, Y18F, 100 mM for HheG G20A) or using 1-300 mM azide while keeping the concentration of epoxide **2** constant at 100 mM. Reactions were incubated at 22 °C. Samples were taken after 30-360 s to ensure determination of initial velocities. Analysis of the resulting kinetic data was performed as previously described for specific activity calculation and kinetic data was fitted using the Hill-equation (1) in Origin Pro2021 (see Figures S6 – S9).

$$v_0 = \frac{v_{max} \cdot [S]^n}{K_{50} + [S]^n} \quad (1)$$

Quantitative analysis of dehalogenation activities

Specific activities (U mg^{-1}) in the dehalogenation of haloalcohols 1,3-dichloro-2-propanol (**1f**), 2-chlorocyclohexanol (**2f**) and 1,3-dibromo-2-propanol (**7g**) based on initial reaction rates were determined using the halide release assay [49]. Reactions were performed in duplicate in a total volume of 1 mL containing 10 mM haloalcohol in 25 mM Tris·SO_4 buffer pH 7.0 at 30 °C (HheC and its mutants) or 22 °C (HheG and its mutants) using 10−400 µg mL^{-1} purified enzyme. Sample of 100 µL volume were taken after 30, 60, 180, 270 and 360 s and mixed with 100 µL assay reagent comprising equal volumes of solution I [0.25 M $NH_4Fe(SO_4)_2$ in 9 M HNO_3] and solution II [saturated solution of $Hg(SCN)_2$ in pure ethanol]. Absorbance at 460 nm was measured using a ClarioStar microplate reader. Specific activities were calculated using standard curves for halides Cl^- and Br^- in the range of 0 to 3.3 mM. Chemical background of negative control reactions without enzyme addition was always subtracted. This assay was also used for the determination of kinetic parameters in the dehalogenation of 1,3-dichloro-2-propanol (**1f**) by HheC mutants. Fir this, the same reaction conditions were used as described above with the substrate concentration ranging from 0.01−20 mM. Resulting kinetic data was fitted using the Michaelis-Menten equation (2) in Origin Pro2021 (see Figure S5).

$$v_0 = \frac{v_{max} \cdot [S]}{K_m + [S]} \quad (2)$$

Melting temperature determination

Thermal shift assays were performed using a QuantStudio 1 Real-Time-PCR system (Thermo Fisher Scientific) in MicroAmp Optical reaction tubes (Thermo Fisher Scientific) containing 20 µg protein and 10 µL 50x concentrated SYPRO orange as fluorescent dye (Thermo Fisher Scientific) in TE buffer in a total volume of 50 µL. Fluorescence (excitation: 580±10 nm, emission: 623±14 nm) was monitored upon increasing the temperature from 10 to 90 °C in 0.5 °C increments. The temperature at which the maximum fluorescence change was observed, representing the melting temperature T_m, was calculated using the Protein Thermal Shift software (version 1.4, Thermo Fisher Scientific).

Determination of nucleophile acceptance

Mutants of HheC and HheG were analyzed in epoxide ring opening of glycidyl phenyl ether (**4**) using azide, nitrite, cyanide, cyanate, thiocyanate as well as chloride and bromide as nucleophiles. Each 1 mL reaction contained 10 mM epoxide **4**, 20 mM nucleophile and 150 µg of purified enzyme in 50 mM Tris·SO_4 buffer, pH 7.0. Reactions were carried out at 22 °C (HheG and its mutants) or 30 °C (HheC and its mutants) with shaking at 900 rpm in an Eppendorf ThermoMixer C. Samples were taken after 1 h and 24 h, extracted with an equal volume of *tert*-butyl methyl ether containing 0.1% (v/v) *n*-dodecane as internal standard. Organic phases were dried over $MgSO_4$ and samples were analyzed by achiral GC (see Table S9 for details regarding temperature programs and retention times).

Determination of regio- and enantioselectivity

To determine the regio- and enantioselectivity of HheC and HheG mutants in epoxide ring opening of epichlorohydrin (**1**), cyclohexene oxide (**2**) and styrene oxide (**3**) in comparison to respective wild-type enzymes, reactions of 1 mL volume were performed in 50 mM Tris·SO_4, pH 7.0 containing 10 mM epoxide, 20 mM azide and 10−200 µg purified enzyme. Reactions were incubated at 22 °C (HheG and its mutants) or 30 °C (HheC and its mutants) with shaking at 900 rpm in an Eppendorf ThermoMixer C. Samples were taken after 15 min for epoxide **1**, 30 min for epoxide **3** and 2 h for epoxide **2**, and extracted with an equal volume of *tert*-butyl methyl ether containing 0.1% (v/v) *n*-dodecane as internal standard. Organic phases were dried over $MgSO_4$ and samples were analyzed by achiral and chiral GC (see Table S9 for details regarding temperature programs and retention times).

MD simulations

Parameters for substrates **1** and azide were generated with the antechamber and parmchk2 modules of AMBER20[57] using the 2nd generation of the general amber force-field (GAFF2).[58,59] Partial charges (RESP model)[60] were set to fit the electrostatic potential generated at the HF/6-31G(d) level of theory. The charges were calculated according to the Merz-Singh-Kollman[61,62] scheme using the Gaussian16 software package.[63] The protonation states were predicted using PROPKA.[64,65] The enzyme structures were obtained from the PDB with the code (1PWZ)[17] and cleaned from other non-peptidic molecules to obtain the wild-type (WT) system in a tetrameric oligomerization state. The single mutation F12Y was introduced using the Pymol mutagenesis tool. Proteins were solvated in a pre-equilibrated truncated octahedral box of 12 Å edge distance using the OPC water model, resulting in the addition of *ca.* 21.300 water molecules, and neutralized by the addition of explicit counterions (*i.e.*, Na^+) using the AMBER20 leap module. All MD simulations were performed using the amber19 force field (ff19SB)[67] in our in-house GPU cluster, GALATEA.

The Pmemd.cuda program from Amber20 was used to perform a two-stage geometry optimization. In the first stage, solvent molecules and ions were minimized, while solute molecules were restrained using 500 kcal·mol^{-1}·$Å^{-2}$ harmonic positional restraints. In the second stage, an unrestrained minimization was performed. The systems were then gradually heated by increasing the temperature by 50 K during six 20 ps sequential MD simulations (0–300 K) under constant volume. Harmonic restraints of 10 kcal·mol^{-1}·$Å^{-2}$ were applied to the solute, and the Langevin equilibration scheme was used to control and equalize the temperature. The time step was kept at one fs during the heating stages to allow potential inhomogeneities to self-adjust. Each system was then equilibrated without restraints for 2 ns at a constant pressure of 1 atm and temperature of 300 K using a 2 fs time step in the isothermal-isobaric ensemble (NPT). After equilibration, five replicas of 250 ns were run for each system (*i.e.*, 1.25 µs per system and 5 µs in total simulated time) in the canonical ensemble (NVT). MD simulations were analyzed by monomers to make it easier to study, multiplying the simulated time by four. All analysis was done using available Python libraries (pyemma[68], mdtraj[69], and mdanalysis[70]) in a jupyter lab environment.

QM calculations

For the QM cluster model, the atom selection was done following the previous work of Himo's group.[21] The only difference is that we added all backbone atoms for residue 12 (the position that is mutated in variant F12Y), allowing for additional flexibility and ring rotation. Geometry minimizations were performed using Gaussian16[63], using the hybrid density functional theory method B3LYP[71,72], and the 6-31G(d,p) basis set. All energies were calculated by performing single-point calculations on the optimized B3LYP/6-31G(d,p) geometries using the M06-2x[73] functional and Def2TZVPP basis set (M06-2X/Def2TZVPP//B3LYP/6-31G(d,p)). Solvation effects were considered using the SMD solvation model, a variation of Truhlar's and coworkers' integral equation formalism variant (IEFPCM)[74], using diethyl ether as solvent.

Shortest Path Map calculations

The Shortest Path Map (SPM) analysis[52,74] was performed using the MD simulations of HheC wild type and variant F12Y. For SPM calculation, the MD simulations are used to compute the inter-residue mean distance and correlation matrices. A simplified graph is created using both matrices, in which only the pairs of residues that show a mean distance of less than 6 Å along the MD simulation are connected through a line. The edge connecting both residues is weighted to the Pearson correlation value (d_{ij}=-log $|C_{ij}|$). The residues with more correlated motions, will be connected through a shorter line. The generated graph is further simplified to identify the shortest path lengths. Following this strategy, the residues whose lines in the graph are shorter (*i.e.*, with more correlated movements) and thus, play an important role in the conformational dynamics of an enzyme, are detected. Finally, the generated SPM graph is drawn on the 3D structure of the enzyme.

AUTHOR INFORMATION

Corresponding author

*Anett Schallmey, E-mail: a.schallmey@tu-braunschweig.de

Notes

The authors declare no competing interests.

ACKNOWLEDGEMENT

This work was financially supported by the German Research Foundation (DFG), grant number 437641034.
M. E. and S.O. thank the Generalitat de Catalunya for the consolidated group TCBioSys (SGR 2021 00487), Spanish MICIN for grant projects PID2021-129034NB-I00 and PDC2022-133950-I00. S.O. is grateful to the funding from the European Research Council (ERC) under the European Union's Horizon 2020 research and innovation program (ERC-2015-StG-679001, ERC-2022-POC-101112805, and ERC-2022-CoG-101088032), and the Human Frontier Science Program (HFSP) for project grant RGP0054/2020. M.E. was supported by ERC-StG (ERC-2015-StG-679001) and ERC-POC (ERC-2022-POC-101112805).

REFERENCES

(1) Xu, Q.; Huang, K.-S.; Wang, Y.-F.; Wang, H.-H.; Cui, B.-D.; Han, W.-Y.; Chen, Y.-Z.; Wan, N.-W. Stereodivergent Synthesis of Epoxides and Oxazolidinones via the Halohydrin Dehalogenase-Catalyzed Desymmetrization Strategy. *ACS Catal.* **2022**, *12* (11), 6285–6293. https://doi.org/10.1021/acscatal.2c00718.

(2) Wan, N.; Tian, J.; Zhou, X.; Wang, H.; Cui, B.; Han, W.; Chen, Y. Regioselective Ring-Opening of Styrene Oxide Derivatives Using Halohydrin Dehalogenase for Synthesis of 4-Aryloxazolidinones. *Adv. Synth. Catal.* **2019**, *361* (20), 4651–4655. https://doi.org/10.1002/adsc.201900786.

(3) Elenkov, M. M.; Tang, L.; Meetsma, A.; Hauer, B.; Janssen, D. B. Formation of Enantiopure 5-Substituted Oxazolidinones through Enzyme-Catalysed Kinetic Resolution of Epoxides. *Org. Lett.* **2008**, *10* (12), 2417–2420. https://doi.org/10.1021/ol800698t.

(4) Elenkov, M. M.; Hoeffken, H. W.; Tang, L.; Hauer, B.; Janssen, D. B. Enzyme-Catalyzed Nucleophilic Ring Opening of Epoxides for the Preparation of Enantiopure Tertiary Alcohols. *Adv. Synth. Catal.* **2007**, *349* (14–15), 2279–2285. https://doi.org/10.1002/adsc.200700146.

(5) Lutje Spelberg, J. H.; van Hylckama Vlieg, J. E. T.; Bosma, T.; Kellogg, R. M.; Janssen, D. B. A Tandem Enzyme Reaction to Produce Optically Active Halohydrins, Epoxides and Diols. *Tetrahedron Asymmetry* **1999**, *10* (15), 2863–2870. https://doi.org/10.1016/S0957-4166(99)00308-0.

(6) Elenkov, M. M.; Primožič, I.; Hrenar, T.; Smolko, A.; Dokli, I.; Salopek-Sondi, B.; Tang, L. Catalytic Activity of Halohydrin Dehalogenases towards Spiroepoxides. *Org. Biomol. Chem.* **2012**, *10* (26), 5063–5072. https://doi.org/10.1039/C2OB25470K.

(7) Zhang, F.-R.; Wan, N.-W.; Ma, J.-M.; Cui, B.-D.; Han, W.-Y.; Chen, Y.-Z. Enzymatic Kinetic Resolution of Bulky Spiro-Epoxyoxindoles via Halohydrin Dehalogenase-Catalyzed Enantio- and Regioselective Azidolysis. *ACS Catal.* **2021**, *11* (15), 9066–9072. https://doi.org/10.1021/acscatal.1c02345.

(8) An, M.; Liu, W.; Zhou, X.; Ma, R.; Wang, H.; Cui, B.; Han, W.; Wan, N.; Chen, Y. Highly α-Position Regioselective Ring-Opening of Epoxides Catalyzed by Halohydrin Dehalogenase from *Ilumatobacter Coccineus*: A Biocatalytic Approach to 2-Azido-2-Aryl-1-Ols. *RSC Adv.* **2019**, *9* (29), 16418–16422. https://doi.org/10.1039/C9RA03774H.

(9) Schallmey, A.; Schallmey, M. Recent Advances on Halohydrin Dehalogenases—from Enzyme Identification to Novel Biocatalytic Applications. *Appl. Microbiol. Biotechnol.* **2016**, *100* (18), 7827–7839. https://doi.org/10.1007/s00253-016-7750-y.

(10) Hasnaoui-Dijoux, G.; Majerić Elenkov, M.; Lutje Spelberg, J. H.; Hauer, B.; Janssen, D. B. Catalytic Promiscuity of Halohydrin Dehalogenase and Its Application in Enantioselective Epoxide Ring Opening. *ChemBioChem* **2008**, *9* (7), 1048–1051. https://doi.org/10.1002/cbic.200700734.

(11) Wang, H.-H.; Wan, N.-W.; Miao, R.-P.; He, C.-L.; Chen, Y.-Z.; Liu, Z.-Q.; Zheng, Y.-G. Identification and Structure Analysis of an Unusual Halohydrin Dehalogenase for Highly Chemo-, Regio- and Enantioselective Bio-Nitration of Epoxides. *Angew. Chem. Int. Ed.* **2022**, *61* (37), e202205790. https://doi.org/10.1002/anie.202205790.

(12) Ma, R.; Hua, X.; He, C.-L.; Wang, H.-H.; Wang, Z.-X.; Cui, B.-D.; Han, W.-Y.; Chen, Y.-Z.; Wan, N.-W. Biocatalytic Thionation of Epoxides for Enantioselective Synthesis of Thiiranes. *Angew. Chem. Int. Ed.* **2022**, *61* (52), e202212589. https://doi.org/10.1002/anie.202212589.

(13) Milčić, N.; Sudar, M.; Dokli, I.; Elenkov, M. M.; Blažević, Z. F. Halohydrin Dehalogenase-Catalysed Synthesis of Enantiopure Fluorinated Building Blocks: Bottlenecks Found and Explained by Applying a

Reaction Engineering Approach. *React. Chem. Eng.* **2023**, *8* (3), 673–686. https://doi.org/10.1039/D2RE00461E.
(14) Zhou, C.; Chen, X.; Lv, T.; Han, X.; Feng, J.; Liu, W.; Wu, Q.; Zhu, D. Flipping the Substrate Creates a Highly Selective Halohydrin Dehalogenase for the Synthesis of Chiral 4-Aryl-2-Oxazolidinones from Readily Available Epoxides. *ACS Catal.* **2023**, *13* (7), 4768–4777. https://doi.org/10.1021/acscatal.2c06417.
(15) van Hylckama Vlieg, J. E. T.; Tang, L.; Lutje Spelberg, J. H.; Smilda, T.; Poelarends, G. J.; Bosma, T.; van Merode, A. E. J.; Fraaije, M. W.; Janssen, D. B. Halohydrin Dehalogenases Are Structurally and Mechanistically Related to Short-Chain Dehydrogenases/Reductases. *J. Bacteriol.* **2001**, *183* (17), 5058–5066. https://doi.org/10.1128/JB.183.17.5058-5066.2001.
(16) Kavanagh, K. L.; Jörnvall, H.; Persson, B.; Oppermann, U. Medium- and Short-Chain Dehydrogenase/Reductase Gene and Protein Families. *Cell. Mol. Life Sci.* **2008**, *65* (24), 3895. https://doi.org/10.1007/s00018-008-8588-y.
(17) de Jong, R. M.; Tiesinga, J. J. W.; Rozeboom, H. J.; Kalk, K. H.; Janssen, D. B.; Dijkstra, B. W. Structure and Mechanism of a Bacterial Haloalcohol Dehalogenase: A New Variation of the Short-Chain Dehydrogenase/Reductase Fold without an NAD(P)H Binding Site. *EMBO J.* **2003**, *22* (19), 4933–4944. https://doi.org/10.1093/emboj/cdg479.
(18) Schallmey, M.; Koopmeiners, J.; Wells, E.; Wardenga, R.; Schallmey, A. Expanding the Halohydrin Dehalogenase Enzyme Family: Identification of Novel Enzymes by Database Mining. *Appl. Environ. Microbiol.* **2014**, *80* (23), 7303–7315. https://doi.org/10.1128/AEM.01985-14.
(19) Koopmeiners, J.; Halmschlag, B.; Schallmey, M.; Schallmey, A. Biochemical and Biocatalytic Characterization of 17 Novel Halohydrin Dehalogenases. *Appl. Microbiol. Biotechnol.* **2016**, *100* (17), 7517–7527. https://doi.org/10.1007/s00253-016-7493-9.
(20) Koopmeiners, J.; Diederich, C.; Solarczek, J.; Voß, H.; Mayer, J.; Blankenfeldt, W.; Schallmey, A. HheG, a Halohydrin Dehalogenase with Activity on Cyclic Epoxides. *ACS Catal.* **2017**, *7* (10), 6877–6886. https://doi.org/10.1021/acscatal.7b01854.
(21) Hopmann, K. H.; Himo, F. Cyanolysis and Azidolysis of Epoxides by Haloalcohol Dehalogenase: Theoretical Study of the Reaction Mechanism and Origins of Regioselectivity. *Biochemistry* **2008**, *47* (17), 4973–4982. https://doi.org/10.1021/bi800001r.
(22) Senthilnathan, D.; Tamilmani, V.; Venuvanalingam, P. Biocatalysis of Azidolysis of Epoxides: Computational Evidences on the Role of Halohydrin Dehalogenase (HheC). *J. Chem. Sci.* **2011**, *123* (3), 279–290. https://doi.org/10.1007/s12039-011-0082-7.
(23) Watanabe, F.; Yu, F.; Ohtaki, A.; Yamanaka, Y.; Noguchi, K.; Yohda, M.; Odaka, M. Crystal Structures of Halohydrin Hydrogen-Halide-Lyases from *Corynebacterium* Sp. N-1074. *Proteins Struct. Funct. Bioinforma.* **2015**, *83* (12), 2230–2239. https://doi.org/10.1002/prot.24938.
(24) Wu, Z.; Deng, W.; Tong, Y.; Liao, Q.; Xin, D.; Yu, H.; Feng, J.; Tang, L. Exploring the Thermostable Properties of Halohydrin Dehalogenase from *Agrobacterium Radiobacter* AD1 by a Combinatorial Directed Evolution Strategy. *Appl. Microbiol. Biotechnol.* **2017**, *101* (8), 3201–3211. https://doi.org/10.1007/s00253-017-8090-2.
(25) Wan, N.-W.; Liu, Z.-Q.; Xue, F.; Shen, Z.-Y.; Zheng, Y.-G. A One-Step Biocatalytic Process for (S)-4-Chloro-3-Hydroxybutyronitrile Using Halohydrin Dehalogenase: A Chiral Building Block for Atorvastatin. *ChemCatChem* **2015**, *7* (16), 2446–2450. https://doi.org/10.1002/cctc.201500453.
(26) Staar, M.; Staar, S.; Schallmey, A. Crystal Contact Engineering for Enhanced Cross-Linking Efficiency of HheG Crystals. *Catalysts* **2022**, *12* (12), 1553. https://doi.org/10.3390/catal12121553.
(27) Staar, M.; Henke, S.; Blankenfeldt, W.; Schallmey, A. Biocatalytically Active and Stable Cross-Linked Enzyme Crystals of Halohydrin Dehalogenase HheG by Protein Engineering. *ChemCatChem* **2022**, *14* (9), e202200145. https://doi.org/10.1002/cctc.202200145.
(28) Solarczek, J.; Kaspar, F.; Bauer, P.; Schallmey, A. G-Type Halohydrin Dehalogenases Catalyze Ring Opening Reactions of Cyclic Epoxides with Diverse Anionic Nucleophiles**. *Chem. – Eur. J.* **2022**, *28* (72), e202202343. https://doi.org/10.1002/chem.202202343.
(29) Lutje Spelberg, J. H.; Tang, L.; Kellogg, R. M.; Janssen, D. B. Enzymatic Dynamic Kinetic Resolution of Epihalohydrins. *Tetrahedron Asymmetry* **2004**, *15* (7), 1095–1102. https://doi.org/10.1016/j.tetasy.2004.02.009.
(30) Nakamura, T.; Yu, F.; Mizunashi, W.; Watanabe, I. Microbial Transformation of Prochiral 1, 3-Dichloro-2-Propanol Injo Optically Active 3-Chloro-1, 2-Propanediol. *Agric. Biol. Chem.* **1991**, *55* (7), 1931–1933. https://doi.org/10.1271/bbb1961.55.1931.
(31) Lutje Spelberg, J. H.; Tang, L.; van Gelder, M.; Kellogg, R. M.; Janssen, D. B. Exploration of the Biocatalytic Potential of a Halohydrin Dehalogenase Using Chromogenic Substrates. *Tetrahedron Asymmetry* **2002**, *13* (10), 1083–1089. https://doi.org/10.1016/S0957-4166(02)00222-7.
(32) Hasnaoui, G.; Lutje Spelberg, J. H.; de Vries, E.; Tang, L.; Hauer, B.; Janssen, D. B. Nitrite-Mediated Hydrolysis of Epoxides Catalyzed by Halohydrin Dehalogenase from *Agrobacterium Radiobacter* AD1: A New Tool for the Kinetic Resolution of Epoxides. *Tetrahedron Asymmetry* **2005**, *16* (9), 1685–1692. https://doi.org/10.1016/j.tetasy.2005.03.021.
(33) Elenkov, M. M.; Hauer, B.; Janssen, D. B. Enantioselective Ring Opening of Epoxides with Cyanide Catalysed by Halohydrin Dehalogenases: A New Approach to Non-Racemic β-Hydroxy Nitriles. *Adv. Synth. Catal.* **2006**, *348* (4–5), 579–585. https://doi.org/10.1002/adsc.200505333.
(34) Schallmey, M.; Floor, R. J.; Hauer, B.; Breuer, M.; Jekel, P. A.; Wijma, H. J.; Dijkstra, B. W.; Janssen, D. B. Biocatalytic and Structural Properties of a Highly Engineered Halohydrin Dehalogenase. *ChemBioChem* **2013**, *14* (7), 870–881. https://doi.org/10.1002/cbic.201300005.

(35) Wu, Z.; Deng, W.; Tong, Y.; Liao, Q.; Xin, D.; Yu, H.; Feng, J.; Tang, L. Exploring the Thermostable Properties of Halohydrin Dehalogenase from *Agrobacterium Radiobacter* AD1 by a Combinatorial Directed Evolution Strategy. *Appl. Microbiol. Biotechnol.* **2017**, *101* (8), 3201–3211. https://doi.org/10.1007/s00253-017-8090-2.
(36) Fox, R. J.; Davis, S. C.; Mundorff, E. C.; Newman, L. M.; Gavrilovic, V.; Ma, S. K.; Chung, L. M.; Ching, C.; Tam, S.; Muley, S.; Grate, J.; Gruber, J.; Whitman, J. C.; Sheldon, R. A.; Huisman, G. W. Improving Catalytic Function by ProSAR-Driven Enzyme Evolution. *Nat. Biotechnol.* **2007**, *25* (3), 338–344. https://doi.org/10.1038/nbt1286.
(37) Tang, X.-L.; Ye, G.-Y.; Wan, X.-Y.; Li, H.-W.; Zheng, R.-C.; Zheng, Y.-G. Rational Design of Halohydrin Dehalogenase for Efficient Chiral Epichlorohydrin Production with High Activity and Enantioselectivity in Aqueous-Organic Two-Phase System. *Biochem. Eng. J.* **2020**, *161*, 107708. https://doi.org/10.1016/j.bej.2020.107708.
(38) Solarczek, J.; Klünemann, T.; Brandt, F.; Schrepfer, P.; Wolter, M.; Jacob, C. R.; Blankenfeldt, W.; Schallmey, A. Position 123 of Halohydrin Dehalogenase HheG Plays an Important Role in Stability, Activity, and Enantioselectivity. *Sci. Rep.* **2019**, *9* (1), 5106. https://doi.org/10.1038/s41598-019-41498-2.
(39) Tian, S.; Ge, X.; Yan, Q.; Li, M.; Huang, Q.; Zhang, X.; Ma, M.; Chen, B.; Wang, J. Directed Evolution of Stereoselective Enzymes Meets Click Reactions: Asymmetric Synthesis of Chiral Triazoles Using a Cu(I)-Compatible Halohydrin Dehalogenase. *Green Synth. Catal.* **2024**. https://doi.org/10.1016/j.gresc.2024.01.001.
(40) Estévez-Gay, M.; Iglesias-Fernández, J.; Osuna, S. Conformational Landscapes of Halohydrin Dehalogenases and Their Accessible Active Site Tunnels. *Catalysts* **2020**, *10* (12), 1403. https://doi.org/10.3390/catal10121403.
(41) Püllmann, P.; Ulpinnis, C.; Marillonnet, S.; Gruetzner, R.; Neumann, S.; Weissenborn, M. J. Golden Mutagenesis: An Efficient Multi-Site-Saturation Mutagenesis Approach by Golden Gate Cloning with Automated Primer Design. *Sci. Rep.* **2019**, *9* (1), 10932. https://doi.org/10.1038/s41598-019-47376-1.
(42) Miyazaki, K.; Takenouchi, M. Creating Random Mutagenesis Libraries Using Megaprimer PCR of Whole Plasmid. *BioTechniques* **2002**, *33* (5), 1033–1038. https://doi.org/10.2144/02335st03.
(43) Gul, I.; Fantaye Bogale, T.; Deng, J.; Wang, L.; Feng, J.; Tang, L. A High-Throughput Screening Assay for the Directed Evolution-Guided Discovery of Halohydrin Dehalogenase Mutants for Epoxide Ring-Opening Reaction. *J. Biotechnol.* **2020**, *311*, 19–24. https://doi.org/10.1016/j.jbiotec.2020.02.007.
(44) Tang, L.; Li, Y.; Wang, X. A High-Throughput Colorimetric Assay for Screening Halohydrin Dehalogenase Saturation Mutagenesis Libraries. *J. Biotechnol.* **2010**, *147* (3), 164–168. https://doi.org/10.1016/j.jbiotec.2010.04.002.
(45) Kaspar, F. Quality Data from Messy Spectra: How Isometric Points Increase Information Content in Highly Overlapping Spectra. *ChemBioChem* **2023**, *24* (7), e202200744. https://doi.org/10.1002/cbic.202200744.
(46) Kaspar, F.; Seeger, M.; Westarp, S.; Köllmann, C.; Lehmann, A. P.; Pausch, P.; Kemper, S.; Neubauer, P.; Bange, G.; Schallmey, A.; Werz, D. B.; Kurreck, A. Diversification of 4′-Methylated Nucleosides by Nucleoside Phosphorylases. *ACS Catal.* **2021**, *11* (17), 10830–10835. https://doi.org/10.1021/acscatal.1c02589.
(47) Eilert, L.; Schallmey, A.; Kaspar, F. UV-Spectroscopic Detection of (Pyro-)Phosphate with the PUB Module. *Anal. Chem.* **2022**, *94* (8), 3432–3435. https://doi.org/10.1021/acs.analchem.1c05356.
(48) Jörnvall, H.; Persson, B.; Krook, M.; Atrian, S.; Gonzalez-Duarte, R.; Jeffery, J.; Ghosh, D. Short-Chain Dehydrogenases/Reductases (SDR). *Biochemistry* **1995**, *34* (18), 6003–6013. https://doi.org/10.1021/bi00018a001.
(49) Bergmann, J. G.; Sanik, John. Determination of Trace Amounts of Chlorine in Naphtha. *Anal. Chem.* **1957**, *29* (2), 241–243. https://doi.org/10.1021/ac60122a018.
(50) Ribas de Pouplana, L.; Fothergill-Gilmore, L. A. The Active Site Architecture of a Short-Chain Dehydrogenase Defined by Site-Directed Mutagenesis and Structure Modeling. *Biochemistry* **1994**, *33* (23), 7047–7055. https://doi.org/10.1021/bi00189a005.
(51) Casadevall, G.; Casadevall, J.; Duran, C.; Osuna, S. The Shortest Path Method (SPM) Webserver for Computational Enzyme Design. *Protein Eng. Des. Sel.* **2024**.
(52) Osuna, S. The Challenge of Predicting Distal Active Site Mutations in Computational Enzyme Design. *Wiley Interdiscip. Rev. Comput. Mol. Sci.* **2021**, *11* (3), e1502.
(53) Wang, H.-H.; Wan, N.-W.; Miao, R.-P.; He, C.-L.; Chen, Y.-Z.; Liu, Z.-Q.; Zheng, Y.-G. Identification and Structure Analysis of an Unusual Halohydrin Dehalogenase for Highly Chemo-, Regio- and Enantioselective Bio-Nitration of Epoxides. *Angew. Chem.* **2022**, *134* (37), e202205790. https://doi.org/10.1002/ange.202205790.
(54) Froger, A.; Hall, J. E. Transformation of Plasmid DNA into E. Coli Using the Heat Shock Method. *J. Vis. Exp. JoVE* **2007**, No. 6, 253. https://doi.org/10.3791/253.
(55) Van Die, I. M.; Bergmans, H. E. N.; Hoekstra, W. P. M. Transformation In *Escherichia Coli*: Studies On The Role Of The Heat Shock In Induction Of Competence. *Microbiology* **1983**, *129* (3), 663–670. https://doi.org/10.1099/00221287-129-3-663.
(56) Gasteiger, E.; Hoogland, C.; Gattiker, A.; Duvaud, S.; Wilkins, M. R.; Appel, R. D.; Bairoch, A. Protein Identification and Analysis Tools on the ExPASy Server. In *The Proteomics Protocols Handbook*; Walker, J. M., Ed.; Springer Protocols Handbooks; Humana Press: Totowa, NJ, 2005; pp 571–607. https://doi.org/10.1385/1-59259-890-0:571.
(57) Case, D. A.; KB, I.; Ben-Shalom, S. R.; Brozell, D. S.; Cerutti III, T. E.; Cheatham III, V. W. D.; Cruzeiro, T. A.; Darden, R. E.; Duke, G. G.; Gilson, M. K. DMY and PAK Amber 2020. *Univ. Calif. San Franc.* **2020**.

(58) Wang, J.; Wolf, R. M.; Caldwell, J. W.; Kollman, P. A.; Case, D. A. Development and Testing of a General Amber Force Field. *J. Comput. Chem.* **2004**, *25* (9), 1157–1174. https://doi.org/10.1002/jcc.20035.
(59) Case, D. A.; Cerutti, D.; Cheateham, T.; Darden, T.; Duke, R.; Giese, T.; Gohlke, H.; Goetz, A. W.; Greene, D.; Homeyer, N. AMBER16 Package. *Univ. Calif. San Franc. CA USA* **2016**.
(60) Bayly, C. I.; Cieplak, P.; Cornell, W.; Kollman, P. A. A Well-Behaved Electrostatic Potential Based Method Using Charge Restraints for Deriving Atomic Charges: The RESP Model. *J. Phys. Chem.* **1993**, *97* (40), 10269–10280. https://doi.org/10.1021/j100142a004.
(61) Singh, U. C.; Kollman, P. A. An Approach to Computing Electrostatic Charges for Molecules. *J. Comput. Chem.* **1984**, *5* (2), 129–145. https://doi.org/10.1002/jcc.540050204.
(62) Besler, B. H.; Merz Jr., K. M.; Kollman, P. A. Atomic Charges Derived from Semiempirical Methods. *J. Comput. Chem.* **1990**, *11* (4), 431–439. https://doi.org/10.1002/jcc.540110404.
(63) Frisch, M. ea; Trucks, G. W.; Schlegel, H. B.; Scuseria, G. E.; Robb, M. A.; Cheeseman, J. R.; Scalmani, G.; Barone, V.; Petersson, G. A.; Nakatsuji, H. *Gaussian 16, Revision C. 01*; Gaussian, Inc., Wallingford CT, 2016.
(64) Olsson, M. H. M.; Søndergaard, C. R.; Rostkowski, M.; Jensen, J. H. PROPKA3: Consistent Treatment of Internal and Surface Residues in Empirical pKa Predictions. *J. Chem. Theory Comput.* **2011**, *7* (2), 525–537. https://doi.org/10.1021/ct100578z.
(65) Søndergaard, C. R.; Olsson, M. H. M.; Rostkowski, M.; Jensen, J. H. Improved Treatment of Ligands and Coupling Effects in Empirical Calculation and Rationalization of pKa Values. *J. Chem. Theory Comput.* **2011**, *7* (7), 2284–2295. https://doi.org/10.1021/ct200133y.
(66) Tian, C.; Kasavajhala, K.; Belfon, K. A. A.; Raguette, L.; Huang, H.; Migues, A. N.; Bickel, J.; Wang, Y.; Pincay, J.; Wu, Q.; Simmerling, C. ff19SB: Amino-Acid-Specific Protein Backbone Parameters Trained against Quantum Mechanics Energy Surfaces in Solution. *J. Chem. Theory Comput.* **2020**, *16* (1), 528–552. https://doi.org/10.1021/acs.jctc.9b00591.
(67) Scherer, M. K.; Trendelkamp-Schroer, B.; Paul, F.; Pérez-Hernández, G.; Hoffmann, M.; Plattner, N.; Wehmeyer, C.; Prinz, J.-H.; Noé, F. PyEMMA 2: A Software Package for Estimation, Validation, and Analysis of Markov Models. *J. Chem. Theory Comput.* **2015**, *11* (11), 5525–5542. https://doi.org/10.1021/acs.jctc.5b00743.
(68) McGibbon, R. T.; Beauchamp, K. A.; Harrigan, M. P.; Klein, C.; Swails, J. M.; Hernández, C. X.; Schwantes, C. R.; Wang, L.-P.; Lane, T. J.; Pande, V. S. MDTraj: A Modern Open Library for the Analysis of Molecular Dynamics Trajectories. *Biophys. J.* **2015**, *109* (8), 1528–1532. https://doi.org/10.1016/j.bpj.2015.08.015.
(69) Gowers, R. J.; Linke, M.; Barnoud, J.; Reddy, T. J. E.; Melo, M. N.; Seyler, S. L.; Domański, J.; Dotson, D. L.; Buchoux, S.; Kenney, I. M.; Beckstein, O. MDAnalysis: A Python Package for the Rapid Analysis of Molecular Dynamics Simulations. *Proc. 15th Python Sci. Conf.* **2016**, 98–105. https://doi.org/10.25080/Majora-629e541a-00e.
(70) Becke, A. D. Density-functional Thermochemistry. I. The Effect of the Exchange-only Gradient Correction. *J. Chem. Phys.* **1992**, *96* (3), 2155–2160. https://doi.org/10.1063/1.462066.
(71) Stephens, P. J.; Devlin, F. J.; Chabalowski, C. F.; Frisch, M. J. Ab Initio Calculation of Vibrational Absorption and Circular Dichroism Spectra Using Density Functional Force Fields. *J. Phys. Chem.* **1994**, *98* (45), 11623–11627.
(72) Zhao, Y.; Truhlar, D. G. The M06 Suite of Density Functionals for Main Group Thermochemistry, Thermochemical Kinetics, Noncovalent Interactions, Excited States, and Transition Elements: Two New Functionals and Systematic Testing of Four M06-Class Functionals and 12 Other Functionals. *Theor. Chem. Acc.* **2008**, *120* (1–3), 215–241. https://doi.org/10.1007/s00214-007-0310-x.
(73) Marenich, A. V.; Cramer, C. J.; Truhlar, D. G. Universal Solvation Model Based on Solute Electron Density and on a Continuum Model of the Solvent Defined by the Bulk Dielectric Constant and Atomic Surface Tensions. *J. Phys. Chem. B* **2009**, *113* (18), 6378–6396. https://doi.org/10.1021/jp810292n.
(74) Casadevall, G.; Casadevall, J.; Duran, C.; Osuna, S. The Shortest Path Method (SPM) Webserver for Computational Enzyme Design. *Protein Eng. Des. Sel.* **2024**, gzae005. https://doi.org/10.1093/protein/gzae005.